THE JOURNAL OF BIOLOGICAL CHEMISTRY
Vol. 276, No. 9, Issue of March 2, pp. 6378–6391, 2001

Printed in U.S.A.

A Kinetic Model for the Action of a Resistance Efflux Pump*

Received for publication, September 5, 2000, and in revised form, November 21, 2000
Published, JBC Papers in Press, November 28, 2000, DOI 10.1074/jbc.M008105200

Adrian R. Walmsley‡§, Tongqing Zhou¶, M. Ines Borges-Walmsley‡, and Barry P. Rosen¶

From the ‡Division of Infection and Immunity, the Institute of Biomedical and Life Sciences, Robertson Building, The University of Glasgow, Glasgow G11 6NU, Scotland, United Kingdom and the ¶Department of Biochemistry and Molecular Biology, Wayne State University School of Medicine, Detroit, Michigan 48201

ArsA is the catalytic subunit of the arsenical pump, coupling ATP hydrolysis to the efflux of arsenicals through the ArsB membrane protein. It is a paradigm for understanding the structure-function of the nucleotide binding domains (NBD) of medically important efflux pumps, such as P-glycoprotein, because it has two sequence-related, interacting NBD, for which the structure is known. On the basis of a rigorous analysis of the pre-steady-state kinetics of nucleotide binding and hydrolysis, we propose a model in which ArsA alternates between two mutually exclusive conformations as follows: the ArsA^1 conformation in which the A1 site is closed but the A2 site open; and the ArsA^2 conformation, in which the A1 and A2 sites are open and closed, respectively. Antimonite elicits its effects by sequestering ArsA in the ArsA^1 conformation, which catalyzes rapid ATP hydrolysis at the A2 site to drive ArsA between conformations that have high (nucleotide-bound ArsA) and low affinity (nucleotide-free ArsA) for Sb(III). ArsA potentially utilizes this process to sequester Sb(III) from the medium and eject it into the channel of ArsB.

One of the most frequently employed strategies to gain resistance to cytotoxic compounds in both eukaryotes and prokaryotes is the active extrusion of these compounds from the cell to reduce the intracellular concentration to subtoxic levels (1). Protein pumps that span the membrane catalyze this extrusion process, and many of them belong to the ATP-binding cassette (ABC)[1] superfamily (2). This family includes the human multidrug resistance P-glycoprotein, which confers resistance to anti-cancer drugs (2), and homologues from bacteria (3, 4), fungi (5), and protozoa (6). Generally, these ABC transporters are composed of two homologous halves, each containing two parts as follows: a transmembrane domain putatively arranged into 6 α-helices and a nucleotide binding domain (NBD).

Our understanding of the mode of operation of these efflux pumps is still rudimentary, and several fundamental questions concerning their function need to be answered if we are to design inhibitors that block these pumps, allowing us to overcome multidrug resistance. For example, since most, if not all, ABC drug transporters have two nucleotide-binding sites (NBS), it is of importance to determine whether these sites are functionally equivalent. Biochemical studies of P-glycoprotein indicate that both NBS can hydrolyze ATP, but substrate-stimulated ATPase activity requires interaction between the two halves of the molecule (7). Inactivation by chemical modification or mutagenesis of either NBS causes a loss of activity, suggesting cooperativity between the sites (8, 9), and it has been suggested that the sites function by an alternating site mechanism (10). P-glycoprotein has been overexpressed and can be purified as a functional ATPase in low concentration of detergent, enabling biophysical studies of the protein (11). The binding of fluorescent analogues of ATP to the protein indicated that there is a single class of site, suggesting that the two NBS are equivalent. Perhaps this is not surprising because the NBS have similar sequences. Although the NBS of P-glycoprotein resemble one another, this is not the case for other mammalian ABC drug transporters, such as multidrug resistance protein 1, and recent studies have shown that the NBS of multidrug resistance protein 1 are nonequivalent (12, 13). Clearly, to understand fully how the NBS interact will require structural information. A recent advance in our understanding has come from the determination, by x-ray crystallography, of the structure of HisP (14, 15), the ATPase subunit of the histidine permease, a bacterial ABC transporter that catalyzes the uptake of histidine. Although arranging the monomeric HisP into a dimer is speculative, the structure predicts that the two nucleotide-binding sites are orientated away from one another. Inactivation of one of these sites results in a transporter that has half the ATPase and transport activity of the wild-type protein complex (16), suggesting that there is little or no cooperativity between these sites. This may represent a real difference with P-glycoprotein, because cross-linking studies have shown that the NBS of P-glycoprotein are in close proximity (17). In addition, the NBD of P-glycoprotein has a site for ligands, such as flavonoids, that modulate drug transport, probably by inhibiting the ATPase activity (18). Unfortunately, we do not have a view of the structure of P-glycoprotein at atomic resolution, and at the present we must glean information from other efflux pumps that have proved more amenable to structure-function studies.

The ArsAB ATPase is a prokaryotic pump that exhibits structural and functional similarity to P-glycoprotein (19). They are both efflux pumps for multiple forms of toxic compounds, have two similar consensus nucleotide binding domains, are substrate-dependent ATPases, have 12 membrane-spanning α-helices arranged in two groups of six, and their NBDs contain allosteric sites. As such, the arsenical pump is a useful model for the study of the molecular mechanism of resistance pumps. However, the arsenical pump is composed of

* This work was supported by United States Public Health Service Grant GM55425 (to B. P. R.), a Wellcome Research Travel Grant from the Burroughs Wellcome Fund, and an award from the NATO Collaborative Research Grant Program, and grants from the BBSRC and Wellcome Trust (to A. R. W.). The costs of publication of this article were defrayed in part by the payment of page charges. This article must therefore be hereby marked "*advertisement*" in accordance with 18 U.S.C. Section 1734 solely to indicate this fact.

§ To whom correspondence and requests for reprints should be addressed. Tel.: 44-141-330-3750; Fax: 44-141-330-3751; E-mail: A.Walmsley@bio.gla.ac.uk.

[1] The abbreviations used are: ABC, ATP-binding cassette; NBD, nucleotide binding domains; MANT, 2′-*O*-(*N*-methylanthraniloyl); NBS, nucleotide-binding sites; MOPS, 4-morpholinepropanesulfonic acid.

two proteins, ArsA and ArsB; ArsA is the 63-kDa catalytic subunit that couples ATP hydrolysis to oxyanion translocation, whereas ArsB is the 45-kDa membrane sector of the pump, a 12-helix protein that acts as the oxyanion-translocating sector of the pump. ArsA is normally bound to ArsB but can be purified as a soluble ATPase in the absence of ArsB, facilitating detailed studies of its structure-function. ArsA is arranged into two homologous halves, the N-terminal (A1) (residues 1–282) and C-terminal (A2) (residues 321–583) domains, which are connected by a flexible 25-residue linker (residues 283–320) (19), and each domain has a consensus NBD. Site-directed mutagenesis of these sequences indicates that both NBDs are required for both catalysis and resistance (20, 21). On the basis of genetic studies, the A1 and A2 NBDs have been shown to interact during catalysis (22, 23) and exhibit strong positive cooperativity (24). The ArsA ATPase is allosterically regulated by its substrate metalloids As(III) and Sb(III) (1). This is similar to the allosteric activation of the P-glycoprotein by drug substrates (1) and may be a common feature of ABC transporters. Indeed, bacterial ABC transporters frequently include ATPase subunits with an allosteric site that controls the ATPase activity (4). In a most important advance, the structure of ArsA has been determined to atomic resolution (25). The structure of ArsA indicates that the A1 and A2 halves of ArsA are arranged into two domains, with the NBS formed from residues contributed from both domains and are located at the interface between them in close proximity to one another. These structural and functional properties of ArsA indicate that the NBS are likely to resemble those in P-glycoprotein and certainly more so than HisP. In common with P-glycoprotein, the NBD of ArsA are in close proximity, face one another, and interactions between them are necessary to support ATPase activity and transport.

Previously, we established that the tryptophan fluorescence of W159H6 ArsA was far more responsive to the binding of the substrate MgATP than the product MgADP, allowing us to exploit this behavior in elucidating the substrate binding, but not the product release, steps of the ATPase mechanism by stopped-flow fluorescence spectroscopy (19, 26, 27). In contrast, the W141H6 ArsA is more responsive to the binding of the product MgADP than the substrate MgATP (28), and here we exploit this behavior in elucidating the product release steps of the ATPase mechanism.

MATERIALS AND METHODS

Purification of His_6-tagged ArsA ATPase—W141H6 ArsA and W159H6 ArsA were purified as described previously (28), quickly frozen, and stored in small aliquots at −80 °C. The concentration of purified ArsA was determined by UV absorbance at 280 nm. The extinction coefficients for W141H6 ArsA and W159H6 ArsA were calculated to be 21,530 and 20,250 M^{-1} cm^{-1}, respectively (28).

Fluorescence Measurements—An Applied Photophysics (London, UK) SX.18MV stopped-flow instrument, operated at 20 °C, was used to monitor ligand-induced changes in the steady-state fluorescence of ArsA with time. For measurements of the change in tryptophan fluorescence, the samples were excited with light at 292.5 nm, selected with a monochromator, and the emission monitored at wavelengths above 335 nm, using a cut-off filter. For measurements of the change in MANT fluorescence, the samples were excited with light at 292.5 nm, selected with a monochromator, and the emission monitored at wavelengths above 420 nm, using a cut-off filter. Invariably, equal volumes of the reactants were mixed together in the stopped-flow instrument, using two syringes of equal volume. The concentration of ArsA was 5 μM, unless otherwise noted, in 50 mM MOPS-KOH (pH 7.5), 0.25 mM EDTA. All concentrations are for the mixing chamber, unless stated otherwise, so that the concentrations in the syringe were twice those quoted for the mixing chamber. The base-line fluorescence was generally set by mixing 5 μM ArsA with buffer and increasing the photomultiplier tube voltage to a level that would give a 4-V signal and ligand-induced changes in fluorescence measured relative to this signal (*i.e.* an increase in the signal from 4 to 4.1 V would correspond to a 2.5% increase in fluorescence and from 4 to 3.9 V a 2.5% quench in fluorescence). Since some of the experiments were conducted over a long time base, we decided to test for photobleaching of the protein by monitoring the fluorescence of ArsA, mixed with buffer in the stopped-flow instrument, over 1000 s; no decay in the protein fluorescence was observed over this time. As a routine second check of fluorescence signals that decay over 1000 s, we have closed the lamp shutter during data acquisition for about 100–200 s and then re-opened it before the end of the reaction. In this manner we have been able to check that the signal continues to decay in the absence of light, indicating that it represents a true ligand-induced change in the protein fluorescence rather than photobleaching. Since ADP inner-filter effects would tend to reduce the signal size for the high concentrations of ADP used in some of the assays, we conducted the following experiment to measure the inner-filter effect for a series of ADP concentrations, bovine serum albumin was mixed with increasing concentrations of ADP up to 5 mM, and the drop in base-line signal was recorded. An inner-filter effect was observed, but it was much less severe than observed in a conventional fluorimeter, increasing linearly over the studied range, with concentrations below 5 mM decreasing the base-line signal by less than 10%. The experiment was also repeated with ArsA W159H6, which is optically unresponsive to the binding of ADP (28), indicating a similar inner-filter effect. Accordingly, data points were corrected for this small inner-filter effect.

Data Analysis—Stopped-flow traces, generated using a logarithmic time base (29), were analyzed by fitting to single (*e.g.* $s = A{\cdot}\exp^{-kt}$; where s represents the change in signal (*e.g.* volts or % fluorescence), t the time, A and k the amplitude and rate constant for the signal change, respectively) or multiple exponential functions (*e.g.* $s = A_1{\cdot}\exp^{-k\,(1)t} + A_2{\cdot}\exp^{-k\,(2)t} + A_3{\cdot}\exp^{-k\,(3)t}$, for a triple exponential function) using the nonlinear regression software with the Applied Photophysics stopped-flow. As a guide to the adequacy of a particular equation to define a data set, we increased the number of exponential parameters within the equation until the data points were randomly distributed about the best fit line in a plot of the residual variance. Concentration dependence data were analyzed by nonlinear regression fitting to hyperbolic functions, using SIGMAPLOT 4.0. Kinetic simulations were set up using the program Pro-K (Applied Photophysics), which uses the Marquardt-Levenberg algorithm for global optimization of the reaction parameters.

ATPase Assays—A continuous assay was used to monitor phosphate production by ArsA. Essentially, the absorbance change at 360 nm associated with the phosphorolysis of 2-amino-6-mercapto-7-methylpurine by the inorganic phosphate generated by the ATPase activity was monitored (26). The phosphorolysis reaction was catalyzed by purine nucleotide phosphorylase. The components of the assay were provided as part of an EnzCheck phosphate assay kit (Molecular Probes, Eugene, OR) and used according to the manufacturer's recommendations. Assays were performed in 40 mM Tris-HCl (pH 7.5), 2 mM $MgCl_2$, containing 0.2 mM sodium azide. The change in absorbance with time was measured in a Unicam (UV2) UV-visible spectrometer. Absorbance changes were converted into phosphate concentrations with $\Delta E_{360} = 12$ $mM^{-1}{\cdot}cm^{-1}$. For stopped-flow studies, both syringes contained the components of the reaction kit, but one syringe contained 10 μM ArsA and the other 1 mM MgATP.

RESULTS

MgADP Binding to ArsA—The binding of MgADP to W141H6 ArsA causes a quench in the tryptophan fluorescence of the protein that can be time-resolved by stopped-flow fluorescence spectroscopy. Fig. 1 shows representative stopped-flow records for the mixing of 5 μM W141H6 ArsA with ADP/5 mM $MgCl_2$. In each case the profile was clearly multiphasic, with a very fast ($t_{1/2}$ <2 ms) phase that was well resolved from a slow decay over 1000 s. Overall, the traces could be fitted to a 4-exponential function, indicative of four phases with $t_{1/2}$ <1 ms, $t_{1/2}$ <2 s, $t_{1/2}$ <40 s, and $t_{1/2}$ <400 s, respectively. However, we found that as the ADP concentration was increased a 5-exponential function gave a better fit because of the appearance of a phase with a $t_{1/2}$ <3 ms. Although this phase involved an increase in fluorescence, this was only slight and not well resolved from the very fast decrease in fluorescence at low ADP concentrations.

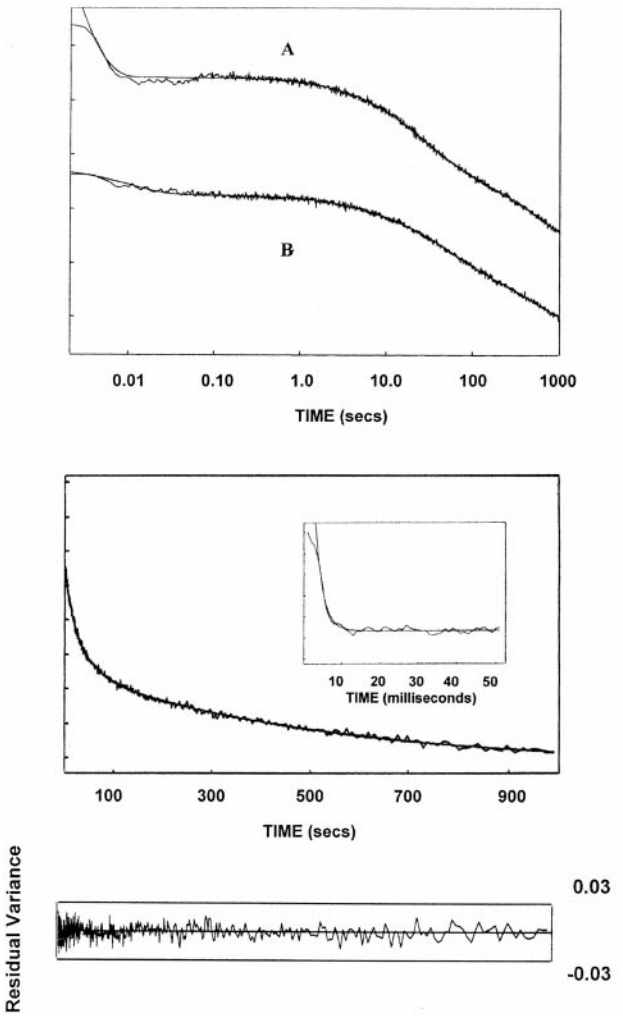

FIG. 1. **MgADP-induced conformational changes in ArsA.** In the *upper panel two* semi-logarithmic plots of stopped-flow traces generated by mixing 5 μM ArsA with 1 mM ADP, 5 mM $MgCl_2$ (*trace A*) and 5 μM ArsA with 0.05 mM ADP, 5 mM $MgCl_2$ (*trace B*) are shown. Changes in the ArsA fluorescence were recorded with Ex = 292.5 nm and Em >335 nm, and one vertical division represents a fluorescence change of 5%. The smooth curve through each trace is the best fit to a 4-exponential equation with rate constants of 510 ($\pm$ 40), 0.14 ($\pm$ 0.02), 0.030 ($\pm$ 0.002), and 0.0020 ($\pm$ 0.0001) s^{-1} (*trace A*); and 84 ($\pm$ 4), 0.20 ($\pm$ 0.02), 0.021 ($\pm$ 0.001), and 0.0020 ($\pm$ 0.0001) s^{-1} (*trace B*)**.** In the *lower panel, trace A* is plotted on a linear time scale, with the first 50 ms of the reaction shown as an *inset.* The smooth curve through the trace is the best fit to the 4-exponential equation defined for *trace A* in the *top panel.* Clearly, the fitted equation provides an adequate fit of the data at both the early and late data points, as indicated by the best fit line and, as shown in the *bottom panel*, a plot of the residual variance of the data about the best fit curve. One vertical division represents a fluorescence change of 2.5% and 1.25% for the *inset.*

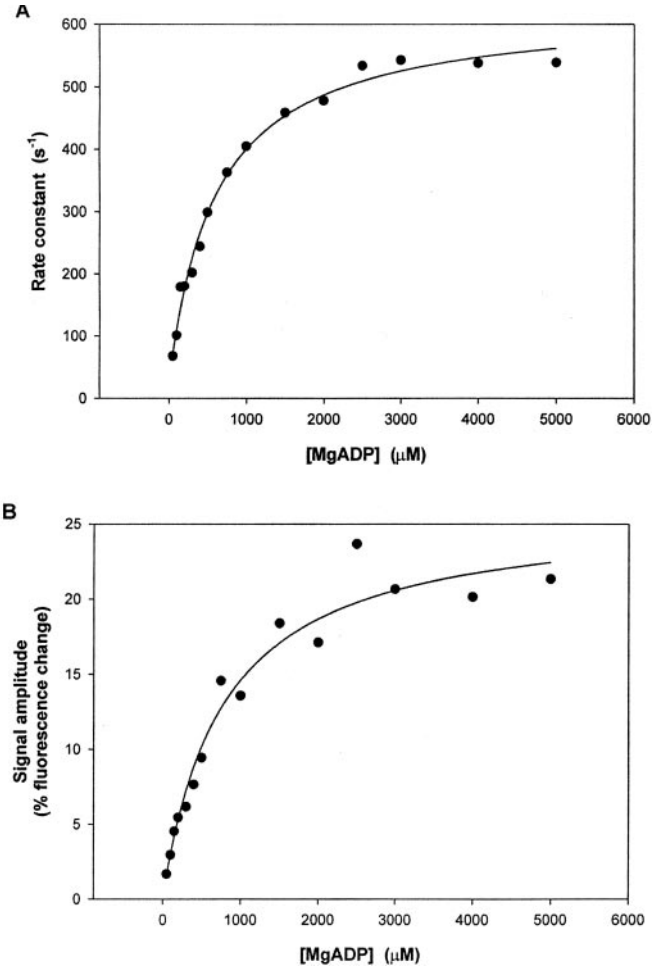

FIG. 2. **The concentration dependence of the rate of binding of MgADP to ArsA.** A series of stopped-flow records were generated by mixing ArsA with 5 mM $MgCl_2$ and ADP, at the indicated concentration, in a stopped-flow device. The rate (*A*) and amplitude (*B*) of the fluorescence signal for the binding of MgADP to ArsA are plotted as a function of the ADP concentration. The curves through the data points are the best fits to a hyperbolic equation, indicating values of 600 ($\pm$ 20) s^{-1}, 30 ($\pm$ 20) s^{-1}, and 600 ($\pm$ 100) μM for k_{max}, k_{min}, and K_d, respectively, in *A*, and of 800 μM ($\pm$ 100) and 26% ($\pm$ 1) for the K_d and maximal fluorescence change (F_{max}) in *B*.

As shown in Fig. 1, only the rate and amplitude of the very fast phase varied with the ADP concentration, indicating that the slower phases were due to isomerizations of the ArsA-ADP complex. The rate constant for the very fast phase increased in a hyperbolic manner with the MgADP concentration (Fig. 2*A*). A fit of the rate data to the following hyperbolic Equation 1,

$$k_{obs} = \frac{k_{max} \cdot [ADP]}{K_d + [ADP]} + k_{min} \qquad \text{(Eq. 1)}$$

indicated maximal (k_{max}) and minimal (k_{min}) rates of binding of 600 ($\pm$ 20) and 30 ($\pm$ 20) s^{-1}, respectively, and a K_d of 600 ($\pm$ 100) μM. This behavior is consistent with the fast phase attributable to a two-step binding process shown in Scheme 1,

$$ArsA^2 + MgADP \underset{k_2[MgADP]}{\overset{k_{-2}}{\rightleftharpoons}} ArsA^3\text{-}MgADP \underset{k_3}{\overset{k_{-3}}{\rightleftharpoons}} ArsA^4\text{-}MgADP$$

SCHEME 1

where the first step is a rapid equilibrium binding of MgADP to ArsA, followed by a rate-limiting isomerization of the ArsA-MgADP complex. Applying Equation 1 to Scheme 1, K_d is equivalent to $1/K_2$ ($= k_{-2}/k_2$), $k_{max} = k_3 + k_{-3}$ and $k_{min} = k_{-3}$. The overall equilibrium constant is a function of both K_2 and K_3 (Equation 2),

$$K_d = \frac{(1/K_2)}{(1 + K_3)} \qquad \text{(Eq. 2)}$$

where K_2 = 0.6 mM and $K_3 = k_3/k_{-3}$ = 600/30 = 20. Thus, the apparent K_d value can be calculated as 24 μM. However, a plot of the amplitude data (Fig. 2*B*), which will provide a measure of the overall K_d, yielded a value of 800 ($\pm$ 100) μM. A plausible explanation for this behavior is that the ArsA exists in two rapidly inter-converting conformational forms that differ in

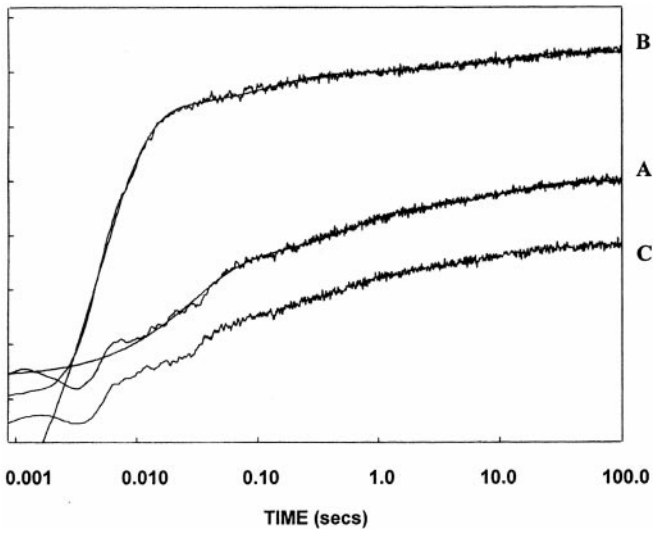

FIG. 3. **The dissociation of the ArsA-MgADP complex induced by MANT-ADP displacement.** Three semi-logarithmic plots of stopped-flow traces generated by mixing 5 μM ArsA, 0.5 mM ADP, 5 mM $MgCl_2$ with 0.125 mM MANT-ADP, 5 mM $MgCl_2$ (*A*); 5 μM ArsA, 5 mM $MgCl_2$ with 0.5 mM ADP, 0.125 mM MANT-ADP, 5 mM $MgCl_2$ (*B*); and 5 μM ArsA, 5 mM $MgCl_2$ with 0.125 mM MANT-ADP, 5 mM $MgCl_2$ (*C*) are shown. Changes in the ArsA fluorescence were recorded with Ex = 292.5 nm and Em > 420 nm, and one vertical division represents a fluorescence change of 2.5%. The smooth curve through *traces A* and *B* are the best fits to a 3-exponential equation with rate constants of 36 (± 1), 1.9 (± 0.1), and 0.09 (± 0.01) s^{-1} (*A*) and 22 (± 2), 7.8 (± 0.3), and 0.094 (± 0.005) s^{-1} (*B*).

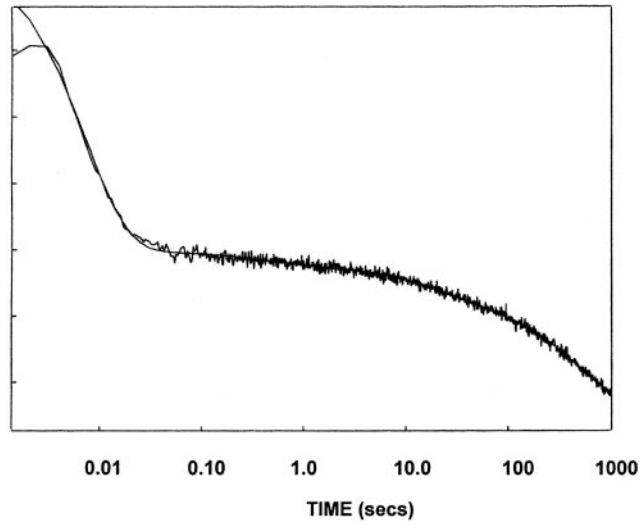

FIG. 4. **Mg^{2+}-induced conformational changes in the ArsA-ADP complex.** A semi-logarithmic plot of a stopped-flow trace generated by mixing 5 μM ArsA, 0.5 mM ADP with 5 mM $MgCl_2$. Changes in the ArsA fluorescence were recorded with Ex = 292.5 nm and Em > 335 nm, and one vertical division represents a fluorescence change of 2.5%. The smooth curve through each trace is the best fit to a 4-exponential equation with rate constants of 139 (± 3), 2.3 (± 0.3), 0.050 (± 0.003), and 0.0020 (± 0.0001) s^{-1}.

their affinities for MgADP (Scheme 2),

$$\mathrm{ArsA^1} \overset{K_1}{\rightleftharpoons} \mathrm{ArsA^2} + \mathrm{MgADP} \overset{K_2}{\rightleftharpoons} \mathrm{ArsA^3\text{-}MgADP} \overset{K_3}{\rightleftharpoons} \mathrm{ArsA^3\text{-}MgADP}$$

SCHEME 2

The overall K_d value is a function of K_1, K_2, and K_3 (Equation 3),

$$K_d = \frac{1}{K_2} \cdot \frac{(1 + K_1)}{(1 + K_3)} \qquad \text{(Eq. 3)}$$

Accordingly, K_1 can be calculated, from the overall K_d and K_2, as 27, indicating that 96% of the ArsA is in the $ArsA^1$ conformation prior to the binding of MgADP.

Dissociation of the ArsA-MgADP Complex—We attempted to measure the rate constant for the dissociation of MgADP from the ArsA-MgADP complex by displacement with MANT-ADP. As shown in Fig. 3*A*, when 5 μM ArsA, 0.5 mM MgADP was mixed with 125 μM MANT-ADP, 5 mM $MgCl_2$ there was an increase in MANT fluorescence, indicating that the ADP had been replaced. However, an identical trace was obtained when the ADP was included with the MANT-ADP (Fig. 3*C*), rather than with the ArsA, during the mixing experiment. This behavior suggests that the ADP can rapidly dissociate from the ArsA and competes with MANT-ADP for binding to ArsA. For this to occur, ADP dissociation must be faster than the binding of MANT-ATP to ArsA (*e.g.* 223 s^{-1} for 125 μM MANT-ATP (Fig. 3*B*)).[2] In contrast, extrapolation of the data in Fig. 2 to the *y* axis suggested a much slower rate of dissociation (*e.g.* k = 30 (± 20) s^{-1}). Conceivably, this might provide a measure of k_{-3} rather than k_{-2} in Scheme 1, but it could also arise if the two NBS had different affinities (see below).

[2] This experiment was repeated for several lower concentrations of ADP with the same result that MgADP dissociation is rapid compared with the rate of binding of MANT-ATP to ArsA.

Mg^{2+} Binding to ArsA-ADP—In a parallel set of experiments, the binding of Mg^{2+} to the W141H6 ArsA-ADP complex was investigated, revealing a similar behavior; formation of the ArsA-MgADP complex led to a fast quench in fluorescence, followed by a slow decay over several minutes (Fig. 4). Only the rate of the fast phase was dependent upon the ADP concentration, suggesting that the three slow phases are attributable to isomerizations of the ArsA-MgADP complex (data not shown). The rate of the fast phase increased in a hyperbolic manner (Fig. 5*A*), deviating only slightly at high concentrations, and the early data points were best fit to a hyperbolic equation with a zero intercept (Equation 4),

$$k_{obs} = \frac{k_{max} \cdot [\mathrm{ADP}]}{K_d + [\mathrm{ADP}]} \qquad \text{(Eq. 4)}$$

Thus, the fit yielded a K_d of 90 (± 10) μM and a maximal rate of binding of 170 (± 10) s^{-1}. This analysis indicated that the back rate, determined from the intercept of the *y* axis, was too slow for accurate determination. A possible explanation for the relatively high affinity binding might be that ADP alone stabilizes the $ArsA^2$ conformation. Consistent with this prediction, the amplitude data indicated a K_d of 190 (± 20) μM and a maximal quench in fluorescence (F_{max}) of 29 (± 1)% (Fig. 5*B*).

The relatively slow rate constant for formation of the ArsA-MgADP complex from ArsA-ADP and Mg^{2+} (*e.g.* k_{max} = 170 (± 10) s^{-1}), as compared with that from ArsA and MgADP (*e.g.* k_{max} = 600 (± 100) s^{-1}), indicates a more complex binding process than the simple addition of Mg^{2+} to the ArsA-ADP complex. The Mg^{2+} cannot bind directly to the $ArsA^2$-ADP complex, nor can complex formation be rate-limited by ADP dissociation from $ArsA^2$, otherwise the rate of complex formation would be independent of the ADP concentration. A plausible explanation of this kinetic behavior is that at sufficiently high concentrations of ADP, when the binding of MgADP would be faster than the dissociation of ADP from the $ArsA^2$-ADP complex, ADP dissociation becomes rate-limiting. Thus interpreting the data implies that ADP dissociates from the ArsA-ADP complex with a rate constant of 170 s^{-1}.

ADP Dissociation from the ArsA-ADP Complex—To test the

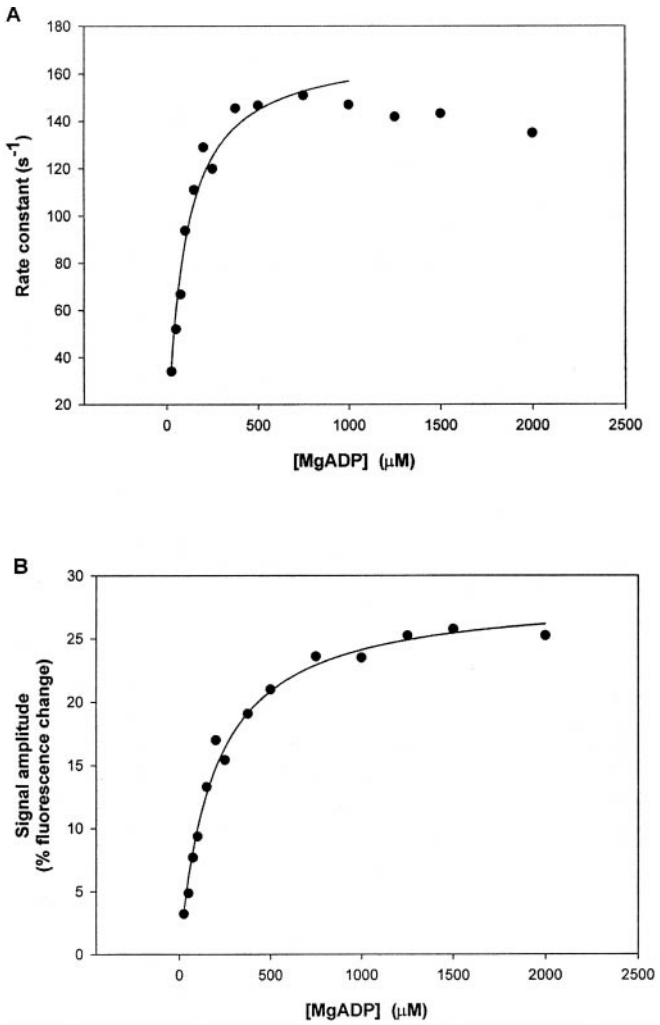

FIG. 5. **The ADP concentration dependence of the rate of formation of the ArsA-MgADP complex induced by the binding of Mg^{2+} to the ArsA-ADP complex.** A series of stopped-flow records were generated by mixing ArsA, equilibrated with ADP at the indicated concentration, with 5 mM $MgCl_2$ in a stopped-flow device. The rate (*A*) and amplitude (*B*) of the fluorescence signal for the formation of the ArsA-MgADP complex are plotted as a function of the ADP concentration. The curves through the data points are the best fits to a hyperbolic equation, indicating values of 170 (± 10) s^{-1} and 90 (± 10) μM for k_{max} and K_d, respectively, in *A*, and of 190 μM (± 20) and 29% (± 1) for the K_d and maximal fluorescence change (F_{max}) in *B*.

prediction that ADP dissociation from ArsA[2] becomes rate-limiting at high ADP concentrations, we attempted to measure the ADP dissociation rate constant, in the absence of Mg^{2+}, by displacement with MANT-ADP. The binding of MANT-ADP to ArsA induced a rapid increase in MANT fluorescence, followed by a slower increase, which was best fit to a 4-exponential function, yielding a rate constant of 350 (± 10) s^{-1} for the fast phase (Fig. 6*A*). In contrast, when ArsA was preincubated with ADP, before mixing with MANT-ADP, only the rapid increase in MANT fluorescence was apparent, although the data were best fit to a double exponential function, with the fast phase occurring with a rate constant of 170 (± 40) s^{-1} (Fig. 6*B*). It is most likely that the difference in reaction profiles is attributable to dissociation of the ArsA-ADP complex rate-limiting the binding of MANT-ADP. A proposal that was supported by the fact that a similar trace to that obtained for the binding of MANT-ADP alone was obtained when ArsA was mixed with MANT-ADP/ADP (Fig. 6*C*). Although, as expected, preincubating the MANT-ADP with ADP caused a reduction in the signal amplitude and yielded a slower rate constant, this is consistent with the ADP competing with the MANT-ADP for binding to ArsA. We conclude that ADP dissociates from ArsA with a rate constant of 170–200 s^{-1}. This conclusion is further supported by the fact that reducing the ADP concentration with which the ArsA was preincubated from 0.5 to 0.25 mM had no effect upon the apparent rate constant for the binding of MANT-ADP (data not shown).

The data presented herein supports the existence of an ArsA-ADP complex, and the value obtained for the rate constant for the dissociation of ADP is comparable with that determined for the maximal rate of formation of the ArsA-MgADP binary complex from ArsA-ADP and Mg^{2+}. Accordingly, this behavior is consistent with the rate-limiting dissociation of ADP from ArsA during the formation of the ArsA-MgADP complex from ArsA-ADP and Mg^{2+}.

Mg^{2+} Dissociation from the ArsA-MgADP Complex—The decrease in the tryptophan fluorescence upon formation of the ArsA-MgADP complex can be reversed by mixing with EDTA, suggesting that ADP is released as EDTA chelates the Mg^{2+}. The stopped-flow trace shown in Fig. 7*B*, for the mixing of 5 μM ArsA, 0.5 mM ADP, 5 mM $MgCl_2$ with 20 mM EDTA, was best fit to a double exponential function, with rate constants of 6.6 and 0.17 s^{-1}, and relative signal amplitudes of 0.9 and 0.1, respectively, giving a total fluorescence change of 22%. This value for the increase in fluorescence is comparable to the decrease in fluorescence for the binding of Mg^{2+} to the ArsA-ADP (*e.g.* 5 μM ArsA/0.5 mM ADP) complex (*cf.* 22 *versus* 21%), indicating that the 20 mM EDTA caused the ArsA-MgADP complex to fully dissociate.[3] The dominant phase, which occurred with a rate constant of 6.6 s^{-1}, must be attributable to the dissociation of the complex because there are no isomerizations of a comparable rate for ternary complex formation from ArsA/ADP and Mg^{2+} (*e.g.* see Fig. 4). The slow rate of dissociation suggests that the ArsA-MgADP complex is relatively stable. Indeed, dilution of the ArsA-MgADP complex, by mixing with buffer in the stopped-flow, was insufficient to dissociate the complex (Fig. 7*E*). These data raise an apparent anomaly because the binding of MgMANT-ADP to ArsA is not rate-limited by the dissociation of the ArsA-MgADP complex (*e.g.* see Fig. 3). A simple explanation for this behavior is that the A1 and A2 NBS have different affinities. EDTA is necessary to induce dissociation of MgADP from the high affinity site, but MANT-ADP can displace MgADP from the low affinity site. Since the tryptophan residue that acts as the reporter of the EDTA effects is positioned in the A1 domain, this suggests that the A1 site has greater affinity than the A2 site.

Sb(III) Binding to ArsA—The binding of Sb(III) to ArsA induced a small quench in the tryptophan fluorescence, indicative of the formation of an ArsA-Sb(III) complex (Fig. 8*A*). The stopped-flow traces were best fit to a triple exponential function with rate constants of about 20, 0.3, and 0.03 s^{-1}, which were independent of the Sb(III) concentration (data not shown). However, a very rapid increase in fluorescence was noted for the higher concentrations of Sb(III) used, which might be due to the binding of Sb(III), followed by three slow isomerizations of the ArsA-Sb(III) complex. A hyperbolic fit of the total amplitude of the signal indicated a K_d of 540 μM and a maximal quench of 5% (data not shown), indicating that Sb(III) is bound with low affinity in the absence of nucleotides (see below).

Sb(III) Binding to the ArsA-MgADP Complex—The binding of Sb(III) to the ArsA-MgADP complex was characterized by a rapid decrease in tryptophan fluorescence (*e.g.* $t_{1/2}$ <50 ms, ΔF <5%), followed by a slow decay in fluorescence over sev-

[3] A signal of comparable amplitude and rate was obtained when 100 mM EDTA was used to induce dissociation of the ArsA-MgADP complex (Fig. 7*A*).

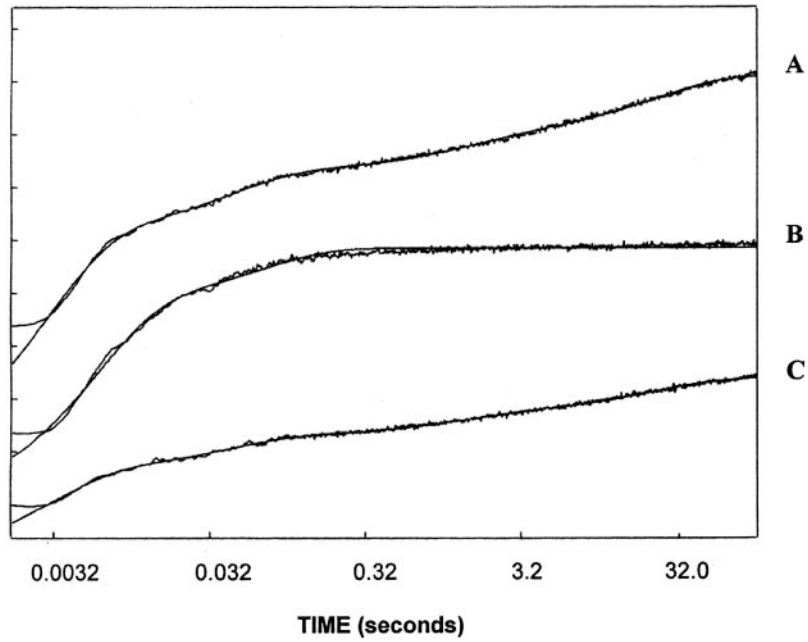

FIG. 6. **The dissociation of the ArsA-ADP complex induced by MANT-ADP displacement.** Three semi-logarithmic plots of stopped-flow traces generated by mixing 5 μM ArsA with 62.5 μM MANT-ADP (*A*), 5 μM ArsA, 0.5 mM ADP with 62.5 μM MANT-ADP (*B*), and 5 μM ArsA with 0.5 mM ADP, 62.5 μM MANT-ADP (*C*) are shown. Changes in the ArsA fluorescence were recorded with Ex = 292.5 nm and Em > 420 nm, and one vertical division represents a fluorescence change of 2.5%. The smooth curve through *traces A* and *C* is the best fit to a 4-exponential equation with rate constants of 400 ($\pm$ 100), 24 ($\pm$ 1), 0.73 ($\pm$ 0.03), and 0.045 ($\pm$ 0.001) s^{-1} (*A*); and 350 ($\pm$ 10), 24 ($\pm$ 1), 0.83 ($\pm$ 0.03), and 0.046 ($\pm$ 0.001) s^{-1} (*C*). The smooth curve through *trace B* is the best fit to a double exponential equation with rate constants of 170 ($\pm$ 40) and 14.8 ($\pm$ 0.4) s^{-1}, where the fast phase represents 78% of the total signal amplitude.

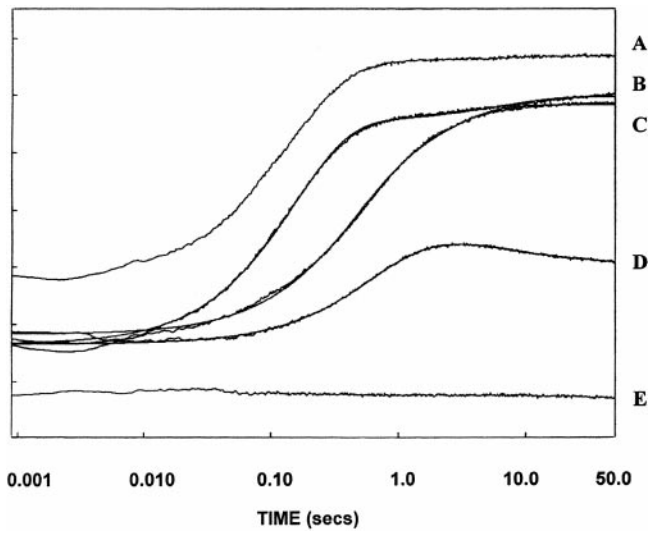

FIG. 7. **EDTA-induced dissociation of the ArsA-MgADP and ArsA-MgADP-Sb(III) complexes.** A set of semi-logarithmic plots of stopped-flow traces generated by mixing 5 μM ArsA, 0.5 mM ADP, 5 mM $MgCl_2$ with 100 mM EDTA (*A*); 5 μM ArsA, 0.5 mM ADP, 5 mM $MgCl_2$ with 20 mM EDTA (*B*); 5 μM ArsA, 0.5 mM ADP, 5 mM $MgCl_2$, 0.1 mM Sb(III) with 20 mM EDTA (*C*); 5 μM ArsA, 0.5 mM ADP, 5 mM $MgCl_2$, 2.5 mM Sb(III) with 20 mM EDTA (*D*); and 5 μM ArsA, 0.5 mM ADP, 5 mM $MgCl_2$ with buffer (*E*) are shown. Changes in the ArsA fluorescence were recorded with Ex = 292.5 nm and Em > 335 nm. One vertical division represents a fluorescence change of 5%. The smooth curves through *traces B* and *C* are the best fits to a double exponential equation with rate constants of 6.60 ($\pm$ 0.02) and 0.170 ($\pm$ 0.004) s^{-1} (*B*); and 2.50 ($\pm$ 0.03) and 0.48 ($\pm$ 0.01) s^{-1} (*C*). The data imply that Sb(III) retards the dissociation of the ArsA-MgADP-Sb(III) complex. Note that *traces A* and *E* are displaced from the other for clarity of presentation.

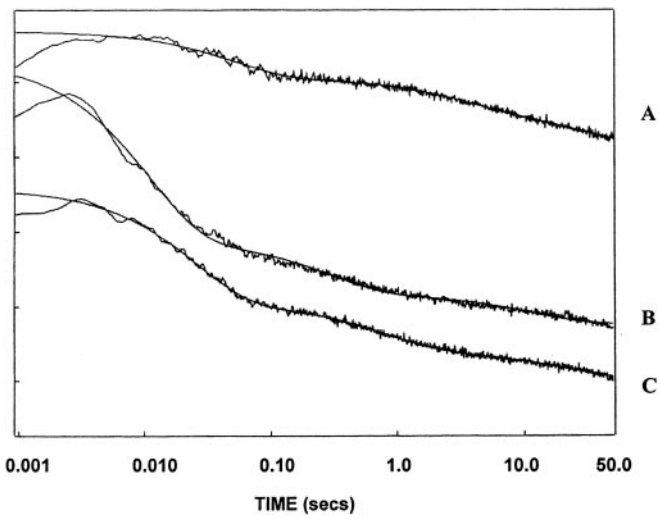

FIG. 8. **Antimonite-induced conformational changes in ArsA and the ArsA-MgADP complex.** A set of semi-logarithmic plots of stopped-flow traces generated by mixing 5 μM ArsA with 2.5 mM Sb(III) (*A*); 5 μM ArsA, 1 mM ADP, 5 mM Mg^{2+} with 1.5 mM Sb(III) (*B*); and 5 μM ArsA, 1 mM ADP, 5 mM Mg^{2+} with 50 μM Sb(III) (*C*), are shown. Changes in the ArsA fluorescence were recorded with Ex = 292.5 nm and Em > 335 nm. One vertical division represents a fluorescence change of 2.5%. The smooth curve through each trace is the best fit to a 3-exponential equation with rate constants of 21 ($\pm$ 1), 0.31 ($\pm$ 0.02), and 0.031 ($\pm$ 0.003) s^{-1} (*A*); 89 ($\pm$ 1), 3.2 ($\pm$ 0.1), and 0.08 ($\pm$ 0.01) s^{-1} (*B*); and 39.1 ($\pm$ 0.4), 1.20 ($\pm$ 0.03), and 0.044 ($\pm$ 0.004) s^{-1} (*C*).

eral minutes (Fig. 8*B*). Sb(III) did not reverse the quench in tryptophan fluorescence caused by the binding of MgADP to ArsA, and we attribute the decrease in fluorescence to the formation of an ArsA-MgADP-Sb(III) complex. Furthermore, as discussed below, EDTA can reverse the quench in fluorescence of this complex, confirming its identity as the ArsA-MgADP-Sb(III) complex. For most stopped-flow traces, the data were adequately fitted to a triple exponential function (*e.g.* Fig. 8*C*), but as the Sb(III) concentration was increased there was a deviation of the early part of the trace from this function (*e.g.* Fig. 8*B*). This is suggestive of the presence of a faster phase, but since this was not well resolved all the traces were fitted to triple exponential functions. As indicated by Fig. 8, *B* and *C*, the most pronounced change, with the Sb(III) concentration, was in the rate and amplitude of the fast phase, and we attribute this phase to the formation of the ArsA-MgADP-Sb(III) complex. The rate of complex formation increased in a hyperbolic manner, and the data were best fit to a hyperbolic equation (*e.g.* Equatrion 1), yielding values for k_{max}, k_{min}, and K_d of 80 ($\pm$ 10) s^{-1}, 3 ($\pm$ 1) s^{-1}, and 60 ($\pm$ 20) μM, respectively (Fig. 9*A*). Applying Equation 2 yielded a value of 2 μM for the overall K_d. On the other hand, a fit of the amplitude data (Fig. 9*B*) to a hyperbolic

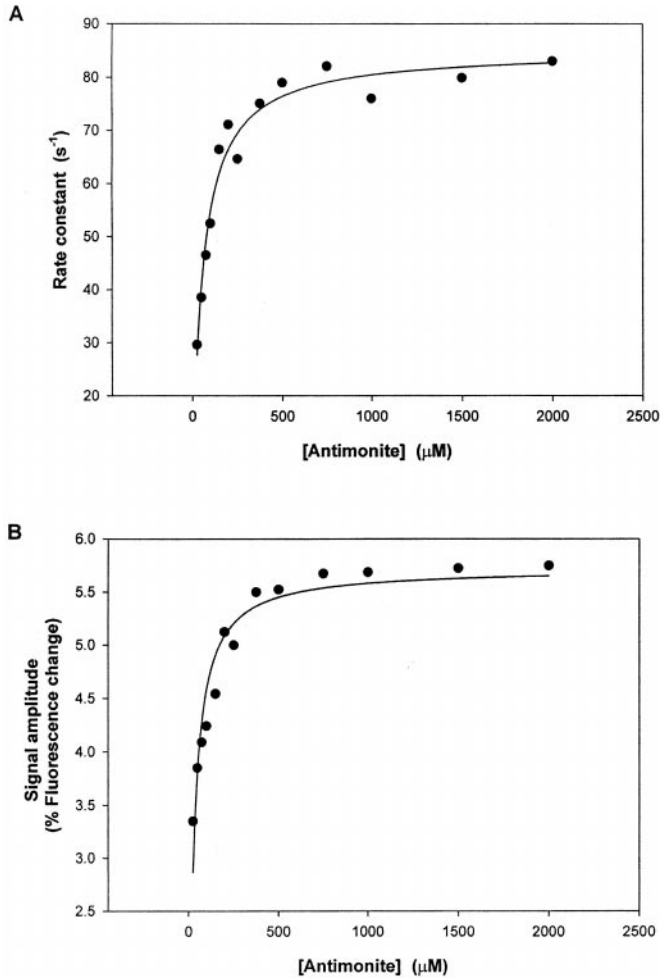

FIG. 9. **The antimonite concentration dependence of the rate and amplitude of the signal associated with formation of the ArsA-MgADP-Sb(III) complex due to the binding of Sb(III) to the ArsA-MgADP complex.** A series of stopped-flow records were generated by mixing ArsA, equilibrated with 1 mM ADP, 5 mM $MgCl_2$, with Sb(III), at the indicated concentration, in a stopped-flow device. The rate (*A*) and amplitude (*B*) of the fluorescence signal for the formation of the ArsA-MgADP-Sb(III) complex are plotted as a function of the antimonite concentration. The curves through the data points are the best fits to a hyperbolic equation, indicating values of 80 (± 10) s^{-1}, 3 (± 1) s^{-1}, and 60 (± 20) μM for k_{max}, k_{min}, and K_d, respectively, in *A*; and of 30 μM (± 3) and 5.7% (± 0.1) for the K_d and maximal fluorescence change (F_{max}) in *B*.

equation yielded an overall K_d of 30 (± 3) μM,[4] suggesting that the ArsA-MgADP complex exists in equilibrium between forms that have high and low affinity (*e.g.* K_1 = 10) for Sb(III). This is perhaps not surprising because the unliganded ArsA exists in two forms that differ in their affinity for MgADP. Although less pronounced, the rates of the intermediate and slow phases increased in a hyperbolic manner with the antimonite concentration, indicating K_d values of 200 (± 100) and 300 (± 100) μM, respectively (data not shown). Previously, we noted that the binding of MgATP to the ArsA-Sb(III) complex caused a triphasic quench in the tryptophan fluorescence of Trp^{159} ArsA; and the rates of the three phases were dependent upon the antimonite concentration, increasing with K_d values of 50 (± 10), 100 (± 30), and 400 (± 100) μM (27).

The kinetics of formation of the ArsA-MgADP-Sb(III) complex are similar to those observed when Sb(III) was mixed with ArsA/MgATP (27). The addition of MgATP to Trp^{159} ArsA caused a transient increase in the tryptophan fluorescence, which we attributed to the build up of the ArsA-MgADP·Pi complex. The addition of Sb(III) to this complex rapidly reversed the fluorescence enhancement, suggesting that Sb(III) caused destabilization of the complex, and the rate of this process increases in a hyperbolic manner with the Sb(III) concentration (*i.e.* k_{max} = 99 s^{-1}; k_{min} = ~1 s^{-1}, and K_d = 330 μM) (27). EDTA was also able to reverse the enhanced fluorescence of this pre-steady-state intermediate, with a rate constant of 4 s^{-1}, confirming that the intermediate was an ArsA-Mg·nucleotide complex that could be destabilized by withdrawing Mg^{2+} (27). Consistent with this interpretation, pre-equilibrating the Trp^{159} ArsA with Sb(III), to form the ArsA-Sb(III) complex, prevented formation of the transient with enhanced fluorescence upon the addition of MgATP. However, in the present investigation with Trp^{141} ArsA, Sb(III) did not reverse the decrease in fluorescence that occurs upon formation of the ArsA-MgADP complex but caused about a further 6% decrease in fluorescence, indicative of the formation of the ArsA-MgADP-Sb(III) complex. This behavior suggests that Sb(III) specifically destabilizes the ArsA-MgADP·P_i complex.

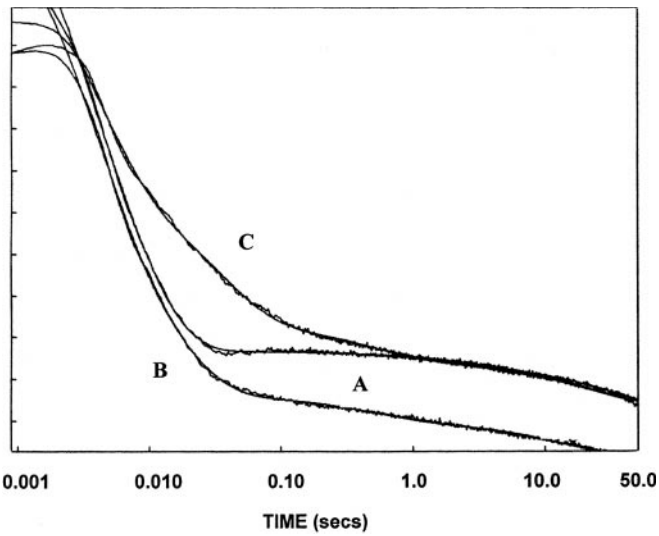

FIG. 10. **The binding of Mg^{2+} to the ArsA-ADP-Sb(III) complex.** A set of semi-logarithmic plots of stopped-flow traces generated by mixing 5 mM Mg^{2+} with 5 μM ArsA, 1 mM ADP, equilibrated with 0 μM Sb(III) (*A*), 25 μM Sb(III) (*B*), and 2500 μM Sb(III) (C) are shown. Changes in the ArsA fluorescence were recorded with Ex = 292.5 nm and Em > 335 nm. One vertical division represents a fluorescence change of 2.5%. The smooth curve through each trace are the best fits to 4-exponential equations yielding rate constants of 460 (± 30), 142 (± 2), and 0.40 (± 0.03), and 0.027 (± 0.003) s^{-1} (*A*); 270 (± 10), 71 (± 2), 2.0 (± 0.1), and 0.067 (± 0.003) s^{-1} (*B*); and 269 (± 4), 30 (± 1), 2.0 (± 0.1), and 0.049 (± 0.002) s^{-1} (*C*). The measured fluorescence changes were 23 (*A*), 25 (*B*), and 22% (*C*).

Mg^{2+} Binding to the ArsA-ADP-Sb(III) Complex—As shown in Fig. 10, there was little difference in the signal amplitudes for the binding of Mg^{2+} to the ArsA-ADP and ArsA-ADP-Sb(III) complexes, apart from a 3% decrease in signal in increasing the Sb(III) concentration from 25 to 2500 μM. These traces indicate that the quench in fluorescence produced by the binding of Sb(III) to ArsA-MgADP is not in fact additive but tends to reduce slightly the overall signal that predominantly arises from the addition of Mg^{2+} to the complex. The formation of the ArsA-MgADP-Sb(III) complex occurred at a slower rate than that of the ArsA-MgADP complex, but there was no apparent dependence upon the Sb(III) concentration, and the rate of the fastest phase varied nonsystematically between 220 and 340 s^{-1} (data not shown).

[4] Since the data were suggestive of tight-binding, we also fitted it to a quadratic equation for a second-order binding process, but this yielded an identical value for the K_d.

Mg^{2+} Dissociation from the ArsA-MgADP-Sb(III) Complex—The effects of Sb(III) upon the rate of MgADP dissociation were investigated by dissociating the ArsA-MgADP complex with EDTA in the presence of Sb(III). The stopped-flow trace shown as Fig. 7*C* indicated that Sb(III) slowed the rate of dissociation of the complex, and the trace was best fit to a double exponential with rate constants of 2.5 and 0.5 s^{-1}, respectively (*cf.* 2.5 *versus* 7 s^{-1}). Although the total signal amplitude was almost equivalent to that in the absence of Sb(III) (*cf.* 20 *versus* 22%), the relative proportions of the two phases had changed to 0.65 and 0.35 for the fast and slow phases, respectively (*cf.* 0.9 and 0.1, respectively, for the ArsA-MgADP complex, Fig. 7*B*). Clearly, the implication is that Sb(III) retards dissociation of Mg^{2+} from the ArsA-MgADP complex. However, we found that the signal amplitude was reduced in the presence of Sb(III). To investigate this phenomena more fully, the experiment was repeated for a series of Sb(III) concentrations. Although the rate constants for the two phases remained constant with increasing antimonite concentrations (*e.g.* phase 1 and 2 varied between 2 and 3 and 0.5–1.5 s^{-1}, respectively; data not shown), the signal amplitude decreased from 22 to 8% in a hyperbolic manner, with a K_d of 260 (± 30) μM[5] (Fig. 11*A*). Although the binding of Sb(III) to the ArsA-MgADP complex induces a quench in the tryptophan fluorescence of the complex, this is less than 6%. Moreover, the binding of Mg^{2+} to the ArsA-ADP and ArsA-ADP-Sb(III) complexes produced a similar quench in protein fluorescence (see Fig. 10). The reduced signal amplitude for the EDTA-induced dissociation of the ArsA-MgADP complex in the presence of Sb(III) cannot simply be accounted for by formation of the ArsA-ADP-Sb(III) complex, with reduced fluorescence, at the end of the reaction. A simple interpretation of this behavior is that the ArsA-MgADP-Sb(III) complex has less MgADP bound at the start of the reaction than the ArsA-MgADP complex. This is probably due to antimonite acting differentially at the two nonequivalent NBS of ArsA, triggering release of MgADP from one site but retarding release from the other site. Consistent with this interpretation, Fig. 11*A* establishes that in the presence of Sb(III) the reduction in signal is attributable to a decrease in the amplitude of the fast phase, rather than an equal reduction in both the fast and slow phases. If the fast and slow phases were attributed to the dissociation of MgADP and a subsequent conformational change in the unliganded ArsA, respectively, then a reduction in the amount of bound MgADP would, as observed, only decrease the amplitude of the fast phase.

Dissociation of the ArsA-MgMANT-ADP Complex—While monitoring the MgADP induced changes in the tryptophan fluorescence of Trp^{141}, ArsA may predominantly report on events occurring at the A1 NBS, studies of the changes in the fluorescence of MANT-ADP have the potential to report on both the A1 and A2 NBS. Consequently, the displacement of MANT-ADP bound to ArsA should resolve both the A1 and A2 NBS if they differ in their affinities. In contrast to the ArsA-MgADP complex, dilution of the ArsA-MgMANT-ADP complex was sufficient to induce its dissociation (Fig. 12*A*, *trace B*), with ADP apparently serving to displace more of the bound MANT-ADP (*e.g.* the signal increased from 11 to 24%; Fig. 12*A*, *trace D*). From a simplistic point of view these results support our hypothesis, with MgMANT-ADP rapidly dissociating from the low affinity site upon dilution, but MgADP displacement needed to dissociate the MgMANT-ADP from the high affinity site. However, the dilution might only be sufficient to dissociate partially the ArsA-Mg·MANT-ATP complex. The dissociation of MANT-ADP was multiphasic, and a 4-exponential equation gave the best fit, indicative of four phases with $t_{1/2}$ ~10, ~50, and ~500 ms and ~9 s, respectively. Only the amplitudes of the fastest two phases increased significantly when ADP was used to dissociate the complex, and we attribute phase 1 and 2 to MANT-ADP dissociation from the low and high affinity sites, respectively. After dilution of the ArsA-MgMANT-ADP complex with buffer the high affinity site would be expected to retain more MANT-ADP than the low affinity site. Consequently, the amplitude of phase 1 would be greater than that of phase 2 after dilution with buffer, but the amplitude of phase 2 should increase after dilution with MgADP. Consistent with this prediction, ADP caused a larger increase in the amplitude of phase 2 (*e.g.* 5-fold) compared with phase 1 (*e.g.* 2-fold), so that the two phases had nearly equal amplitudes (*e.g.* 7.9 and 7.7% fluorescence change for phases 1 and 2, respectively) and

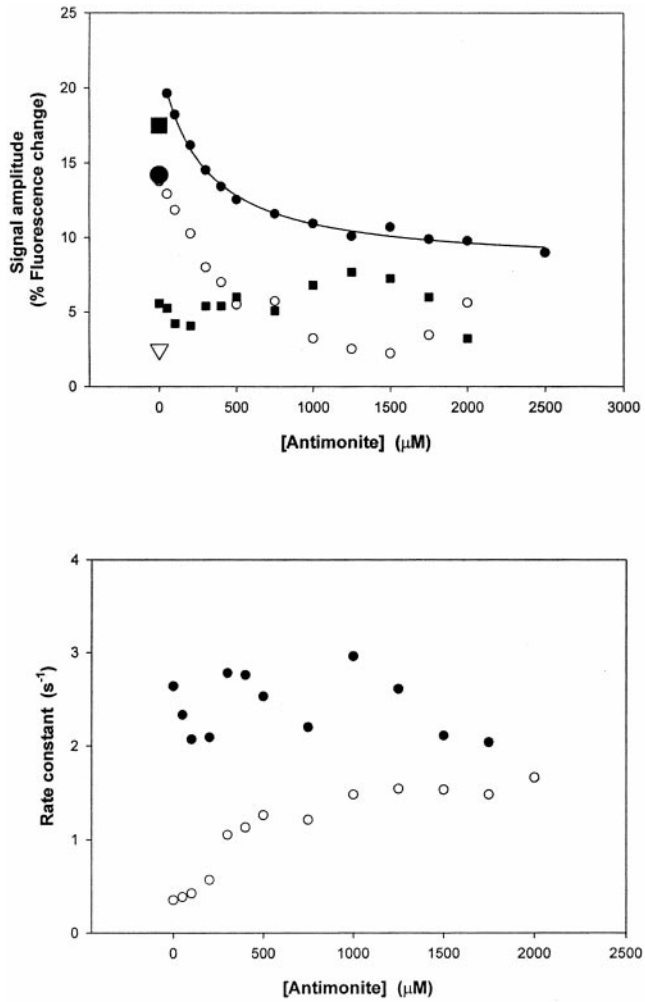

FIG. 11. **The antimonite concentration dependence of the EDTA-induced dissociation of the ArsA-MgADP-Sb(III) complex.** A series of stopped-flow records were generated by mixing by mixing 5 μM ArsA, 0.5 mM ADP, 5 mM $MgCl_2$, equilibrated with the indicated concentrations of Sb(III), with 20 mM EDTA in a stopped-flow device. These traces were fitted to a double exponential equation, and in the *upper panel*, the amplitudes of the fast (○) and slow (■) phases and the total amplitude (●) are plotted as a function of the antimonite concentration. For comparison, the amplitudes of the corresponding phases for the dissociation of the ArsA-MgADP complex in the absence of Sb(III) are shown on the plot as the *large symbols* ●, ▽, ■, respectively. The curve through the data points for the decrease in total amplitude is the best fit to a hyperbolic equation, indicating that the fluorescence decreases from 22 (± 1) to 8.0% (± 0.3) with a K_d 260 μM (± 30). This decrease in fluorescence is clearly attributable to a decrease in the fast phase, with the slow phase remaining constant. In the *lower panel* the corresponding rate constants for the fast (●) and slow (○) phases are shown.

[5] A second set of data yielded a half-saturation constant of 170 μM.

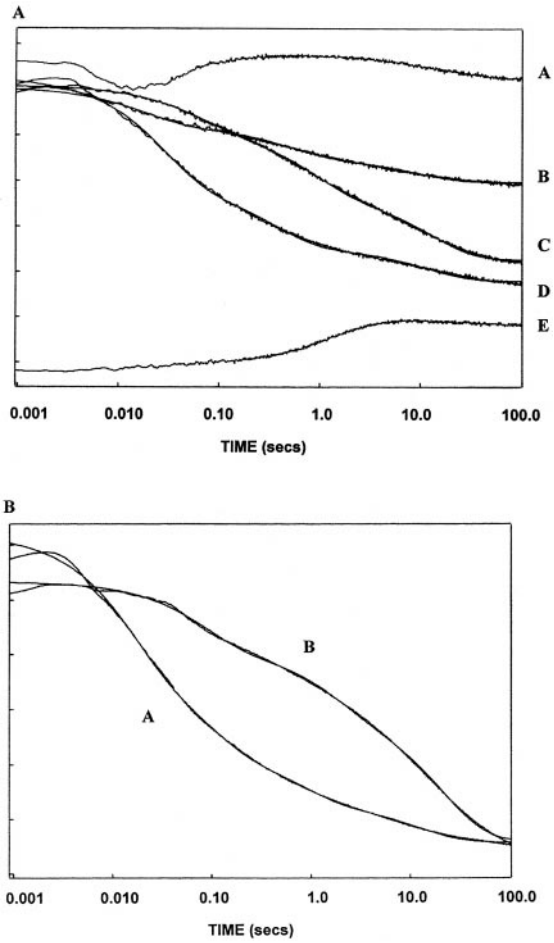

FIG. 12. **Dissociation of the ArsA-MgMANT-ADP complex.** *A,* five semi-logarithmic plots of stopped-flow traces generated by mixing 5 μM ArsA, 25 μM MANT-ADP, 5 mM $MgCl_2$ with 20 mM EDTA (*trace A*); 5 μM ArsA, 25 μM MANT-ADP, 5 mM $MgCl_2$ with buffer (*trace B*); 5 μM ArsA, 25 μM MANT-ADP, 5 mM $MgCl_2$, 0.5 mM Sb(III) with 2.5 mM ADP, 5 mM $MgCl_2$ (*trace C*); 5 μM ArsA, 25 μM MANT-ADP, 5 mM $MgCl_2$ with 2.5 mM ADP, 5 mM $MgCl_2$ (*trace D*); and 5 μM ArsA, 5 mM $MgCl_2$ with 25 μM MANT-ADP, 2.5 mM ADP, 5 mM $MgCl_2$ (*trace E*) are shown. Changes in the ArsA fluorescence were recorded with Ex = 292.5 nm and Em > 420 nm, and one vertical division represents a fluorescence change of 2.5%. The smooth curve through *trace D* is the best fit to a 4-exponential equation with rate constants of 71 ($\pm$ 2) s^{-1} (7.9% fluorescence change), 13.0 ($\pm$ 0.4) s^{-1} (7.7% fluorescence change), 1.50 ($\pm$ 0.04) s^{-1} (4.8% fluorescence change), and 0.060 ($\pm$ 0.001) s^{-1} (3.4% fluorescence change). The curve through *trace B* is a fit to a 4-exponential equation in which the rate constants were held constant at the values derived from *trace D*, so as to allow a comparison of the amplitudes of the four phases in each trace. This procedure yielded amplitudes of 3.5, 1.6, 3.2, and 2.4% for phases 1–4, respectively, for *trace B. Trace C* could be adequately fitted by a triple exponential function, with rate constants of 14.0 ($\pm$ 0.3), 1.10 ($\pm$ 0.02), and 0.080 ($\pm$ 0.001) s^{-1}, as shown by the smooth curve through the trace, indicating the absence of fast phase 1. *B,* two semi-logarithmic plots of stopped-flow traces generated by mixing 50 μM ArsA, 62.5 μM MANT-ADP, 5 mM $MgCl_2$ with 2.5 mM ADP, 5 mM $MgCl_2$ (*A*); and 50 μM ArsA, 62.5 μM MANT-ADP, 5 mM $MgCl_2$, 0.5 mM Sb(III) with 2.5 mM ADP, 5 mM $MgCl_2$ (*B*). The smooth curve through *trace A* is the best fit to a 4-exponential equation with rate constants of 67 ($\pm$ 1), 11.0 ($\pm$ 0.3), 1.30 ($\pm$ 0.03), and 0.080 ($\pm$ 0.002) s^{-1}. *Trace B* could be adequately fitted by a triple exponential function, with rate constants of 12.0 ($\pm$ 0.2), 0.60 ($\pm$ 0.01), and 0.050 ($\pm$ 0.001) s^{-1}, as shown by the smooth curve through the trace, indicating the absence of fast phase 1.

constituted 66% of the total signal. EDTA-induced dissociation of the complex caused a small and rapid decrease in fluorescence but was followed by an increase in fluorescence; we attribute this behavior to the rapid dissociation of the ArsA-MgMANT-ADP complex followed by the re-binding of MANT-ADP to form the ArsA-MANT-ADP complex (Fig. 12*A*, *trace A*).

If antimonite enhances the dissociation of MgADP from one site but retards its dissociation from the other, then we might expect that the rates of phases 1 and 2 observed for MgMANT-ADP dissociation would increase and decrease, respectively. The dissociation of MANT-ADP from the ArsA-MgMANT-ADP-Sb(III) complex was characterized by a 19% decrease in MANT fluorescence that could be adequately fitted to a triple exponential function with similar rate constants to those determined for phases 2–4 in the absence of Sb(III) (Fig. 12*A*, *trace C*). To optimize this analysis, we optimized the signal using a 10-fold higher concentration of ArsA, for which the larger signal could be more clearly resolved into its constituent phases. When 50 μM ArsA, 62.5 μM MANT-ADP, 5 mM $MgCl_2$ was mixed with 2.5 mM ADP, 5 mM $MgCl_2$, the fast phase was clearly resolved into two phases, with rate constants of 67 ($\pm$ 1) and 11.0 ($\pm$ 0.3) s^{-1} (Fig. 12*B, trace A*). In the presence of antimonite the faster of the two phases was clearly absent, and the slower phase occurred with a rate constant of 12.0 ($\pm$ 0.2) s^{-1} (Fig. 12*B*, *trace B*). The effect of antimonite was to abolish the fast phase, and we attribute this behavior to Sb(III)-induced dissociation from the low affinity site. Although complicated by the multiphasic traces, these results are highly consistent with our conclusion that the ArsA NBS are nonequivalent, one site allowing rapid release of nucleotides and the other slow release, and that antimonite acts differentially on these sites causing product dissociation from the low affinity site.

MgADP Binding to the ArsA-Sb(III) Complex—Since our studies indicated that antimonite amplifies the difference in affinities of the two NBS for MgADP, we decided to determine the kinetics of MgADP binding to the ArsA-Sb(III) complex. The binding of (1 mM) MgADP to the ArsA-Sb(III) complex was characterized by a multiphasic decrease in the tryptophan fluorescence of ArsA (Fig. 13). There was a very rapid decrease in fluorescence (*e.g.* phase 1, $t_{1/2}$ <2 ms), which we attribute to the binding of MgADP to the ArsA-Sb(III) complex, followed by a slow decrease over several seconds (*e.g.* phases 3 and 4, $t_{1/2}$ <0.4 and 15 s, respectively). As the Sb(III) concentration was increased we observed the progressive appearance of a phase of intermediate rate (*e.g.* phase 2, $t_{1/2}$ ~10–20 ms). The stopped-flow traces were best fit to a 4-exponential function. As shown in Fig. 14*A*, for increasing Sb(III) concentrations, an increase in the amplitude of phase 2 was concomitant with a decrease in that for phase 4. The amplitude of phase 1 was independent of the Sb(III) concentration, as expected for a fixed MgADP concentration, as was that of phase 3. In contrast, only the rate constants for phases 1 and 3 had a dependence upon the Sb(III) concentration, with those for phase 1 and 3 decreasing and increasing, respectively, with increasing concentration (Fig. 14*B*).

The hyperbolic decrease in the rate of ternary complex formation (*e.g.* phase 1) suggests that the ArsA alternates between conformations that differ in their affinities for Sb(III) and MgADP and that this transition is rate-limiting for formation of the ArsA-MgADP-Sb(III) ternary complex (30, 31). The forward and backward rate constants for the transition and the apparent affinity for Sb(III) can be determined from an inverse hyperbolic function (Equation 5),

$$k_{obs} = k_f + \frac{k_r \cdot K_{app}}{[Sb(III)] + K_{app}} \quad \text{(Eq. 5)}$$

A fit of the phase 1 rate data (●) in Fig. 14*B* to Equation 5 indicated values for k_f, k_r, and K_{app} of 490 ($\pm$ 10) s^{-1}, 310 ($\pm$ 20) s^{-1}, and 140 ($\pm$ 40) μM, respectively. The simplest mechanism consistent with this kinetic behavior would be one in which

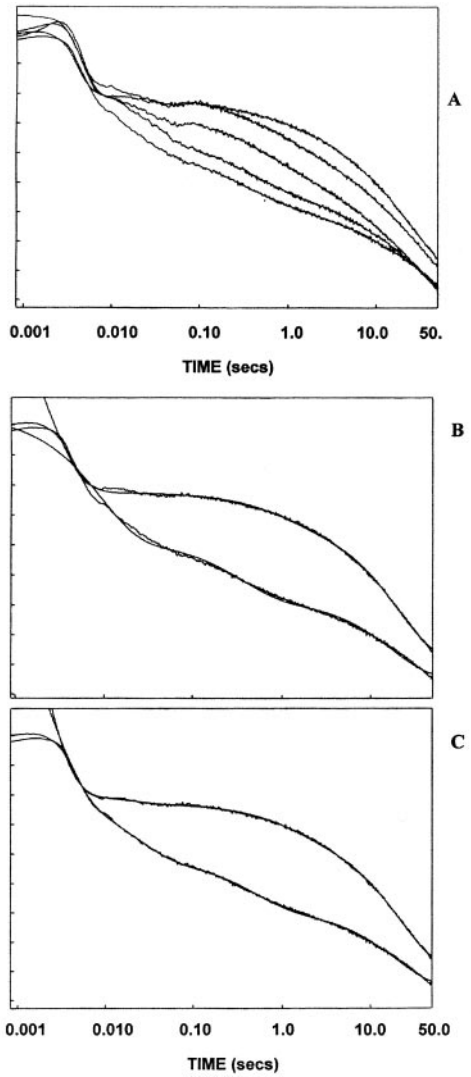

FIG. 13. **The binding of MgADP to the ArsA-Sb(III) complex.** A set of semi-logarithmic plots of stopped-flow traces generated by mixing 5 μM ArsA, 1 mM ADP, 5 mM Mg^{2+} with 25, 100, 150, 200, 375, and 750 μM Sb(III) are shown in *A*. The traces are arranged from top to bottom in order of increasing Sb(III) concentration, with the top trace corresponding to the lowest Sb(III) concentration. Changes in the ArsA fluorescence were recorded with Ex = 292.5 nm and Em > 335 nm. One vertical division represents a fluorescence change of 2.5%. The smooth curve through the traces generated with 25 μM (*top trace*) and 750 μM (*bottom trace*) Sb(III) are the best fits to 3- and 4-exponential equations in *B* and *C*, respectively. For the 3-exponential analyses in *B*, there is clearly a systematic deviation of the fitted curves about the measured curves indicate the inadequacy of this fit to the data. The 4-exponential analyses in *C* yielded rate constants of 740 (± 20), 58 (± 5), 0.770 (± 0.002), and 0.005 (± 0.001) s^{-1} for 25 μM Sb(III); and 460 (± 12), 46 (± 1), 2.060 (± 0.003), and 0.005 (± 0.001) s^{-1} for 750 μM Sb(III).

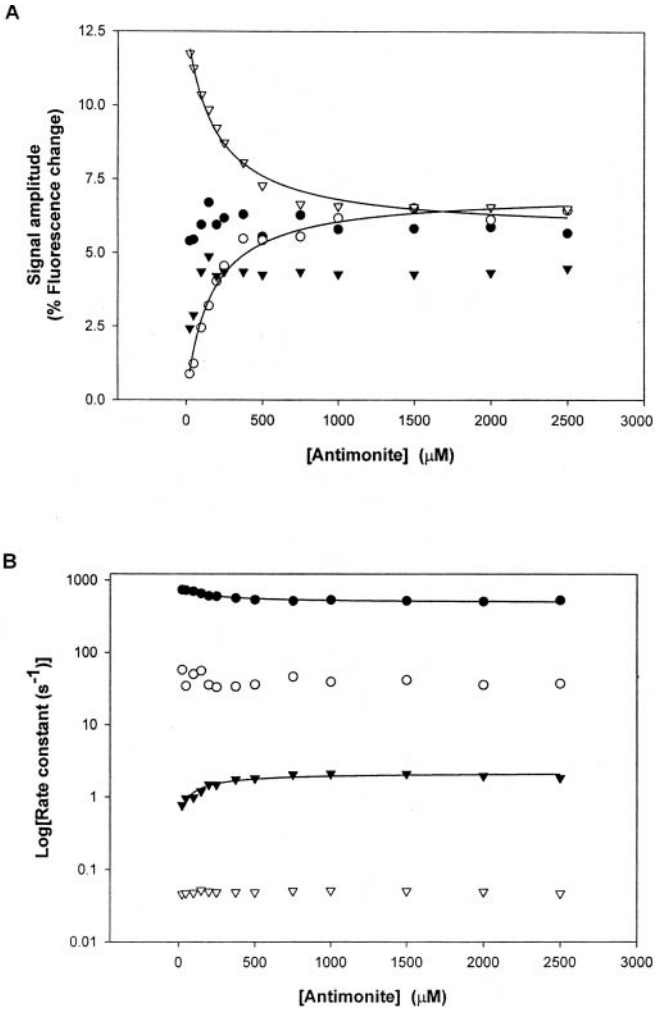

FIG. 14. **The antimonite concentration dependence rate and amplitude of the signal associated with formation of the ArsA-MgADP-Sb(III) complex due to the binding of MgADP to the ArsA-Sb(III) complex.** A series of stopped-flow records were generated by mixing ArsA, equilibrated with the indicated concentrations of Sb(III), with 1 mM ADP, 5 mM $MgCl_2$ in a stopped-flow device. These traces were fitted to a 4-exponential equation, and the amplitude (*A*) and log of the rate (*B*) for each phase are plotted as a function of the antimonite concentration; the symbols used for phases 1–4 are ●, ○, ▽, and ▼, respectively. The curves through the phase 2 (○) and 4 (▼) data points in *A* are the best fits to hyperbolic equations, indicating K_d values of 200 (± 20) and 180 (± 30) μM, respectively. The curves through the phase 1 (●) and 3 (▼) data points in *B* are the best fits to hyperbolic equations (*e.g.* Equations 5 and 1, respectively), indicating values for k_{max} (or k_f), k_{min} (or k_r), and K_d of 490 (± 10) s^{-1}, 310 (± 20) s^{-1}, and 140 (± 40) μM; and 1.7 (± 0.2) s^{-1}, 0.5 (± 0.2) s^{-1}, and 200 (± 100) μM, respectively.

Sb(III) and MgADP compete for binding to ArsA. However, as discussed above, Sb(III) does not reverse the quenched fluorescence of the ArsA-MgADP complex, but subsequent treatment with EDTA does reverse the quench, indicating the formation of an ArsA-MgADP-Sb(III) ternary complex. Moreover, recent crystallographic studies have revealed the existence of the ArsA-MgADP-Sb(III) ternary complex (25). A more elaborate model of ternary complex formation is required, and we propose the following Scheme 3:

$$\begin{array}{ccccc} & & k_{-1} & & k_{-2} & & \\ & & \rightleftarrows & & \rightleftarrows & & \\ ArsA^1 + Sb(III) & & ArsA^1\text{-}Sb(III) & + MgADP & & ArsA^1\text{-}MgADP\text{-}Sb(III) \\ & & k_1 & & k_2 & & \\ k_{-3}\uparrow\downarrow k_3 & & k_{-4}\uparrow\downarrow k_4 & & & k_{-5}\uparrow\downarrow k_5 & \\ & & k_{-6} & & k_{-7} & & \\ & & \rightleftarrows & & \rightleftarrows & & \\ ArsA^2 + Sb(III) & & ArsA^2\text{-}Sb(III) & + MgADP & & ArsA^2\text{-}MgADP\text{-}Sb(III) \\ & & k_6 & & k_7 & & \end{array}$$

SCHEME 3

If $ArsA^1$ has a greater affinity than $ArsA^2$ for Sb(III) (*e.g.* $1/K_1 < 1/K_6$), then the binding of Sb(III) will sequester the ArsA in the $ArsA^1$ conformation. On the other hand, if $ArsA^2$-Sb(III) has a greater affinity than $ArsA^1$-Sb(III) for MgADP, then the binding of MgADP will tend to sequester the ArsA in the $ArsA^2$ conformation. The fact that $ArsA^2$-MgADP-Sb(III) exists implies that $1/K_7 < 1/K_1$. If the transition between $ArsA^1$-Sb(III) and $ArsA^2$-Sb(III) is rate-limiting, then the rate of ternary complex formation (k_{obs}) is approximated by Equation 5, with $k_f \sim k_4$, $k_r \sim k_{-4}$, and $K_{app} \sim K_2$. In the absence of Sb(III) ArsA

exists as an equilibrium mixture of 61% $ArsA^1$-MgADP and 39% $ArsA^2$-MgADP.

The hyperbolic decrease in the rate of phase 1 indicates that the ArsA alternates between conformations that differ in their affinities for antimonite and the nucleotide, and this behavior can be interpreted in terms of Scheme 3, but can this scheme account for the other phases? The rates of phases 2 and 4 are independent of the antimonite concentration, suggesting that these are attributable to isomerizations of the ArsA-MgADP-Sb(III) complex, whereas the rates of phases 1 and 3 are dependent upon the antimonite concentration, suggesting that they are attributes of the binding of antimonite. One possibility is that phase 1 is due to formation of the $ArsA^1$-Sb(III) complex and phase 2 to formation the $ArsA^1$-MgADP-Sb(III) complex. If the $ArsA^1$-Sb(III) and $ArsA^2$-Sb(III) complexes have a similar fluorescence then the amplitude of phase 1 would be independent of the concentration of Sb(III), but the rate would decrease hyperbolically because the $ArsA^2$-Sb(III) to $ArsA^1$-Sb(III) transition is rate-limiting for the binding of Sb(III). On the other hand, if the $ArsA^1$-MgADP-Sb(III) complex has a lower fluorescence than the ArsA-Sb(III) complexes, and our studies indicate that it does, then the amplitude of phase 2 would increase as the concentration of the $ArsA^1$-Sb(III) complex increases with the Sb(III) concentration; and the rate of $ArsA^1$-MgADP-Sb(III) complex formation would be concentration-independent for a fixed concentration of MgADP. Similarly, phases 3 and 4 can be attributed to formation of the $ArsA^2$-Sb(III) and $ArsA^2$-MgADP-Sb(III) complexes. However, the binding of Sb(III) to $ArsA^2$ is probably rate-limited by a slow isomerization following formation of the $ArsA^2$-Sb(III) complex, which is rapid but slower than the $ArsA^1$ to $ArsA^2$ transition. The amplitude of phase 4 decreases with the Sb(III) concentration as more of the ArsA is sequestered in the $ArsA^1$ conformation by Sb(III). Indeed, the decrease in the amplitude of phase 4 mirrors the increase in the amplitude of phase 2, providing strong evidence that Sb(III) pulls ArsA between two mutually exclusive conformations. A consequence of this interpretation is that the rate of phase 1 and the amplitudes of phases 2 and 4 should all be determined by the affinity of $ArsA^2$ for Sb(III) (*e.g.* K_2 in Scheme 3). Consistent with this prediction, fits of the amplitude data for phases 2 and 4 to hyperbolic equations yielded apparent K_d values of 200 (± 20) and 180 (± 30) μM, respectively, which are similar to the value of 140 (± 40) μM obtained from the rate data for phase 1 (Fig. 14). An inconsistency with this interpretation is that in applying Equation 5, a simplifying assumption is made that the $ArsA^2$ state has no affinity for Sb(III), but the rate data for phase 3, which should provide a measure of the affinity of $ArsA^2$ for Sb(III), indicated that this state has moderate affinity for Sb(III) (*e.g.* K_d = 200 (± 100) μM). However, the $ArsA^1$ state need only have a higher affinity than $ArsA^2$ for Sb(III) to sequester the protein in this conformation. This aside, the data clearly indicate that ArsA can adopt different conformations that are stabilized by MgADP and Sb(III) to different extents. We have observed similar kinetic behavior for the binding of Mg^{2+} to the ArsA-ATP-Sb(III) complex, with the rate of formation of the ArsA-ATP-Sb(III) complex decreasing in a hyperbolic manner with increasing Sb(III) concentration (27). Although indicative of the transition between nucleotide and antimonite-stabilized conformations, this transition was much slower (*e.g.* $k_f = 1\ s^{-1}$ and $k_r = 0.5\ s^{-1}$), and the antimonite favored conformation had a higher affinity of 65 μM for antimonite (27).

The Pre-steady-state Production of P_i—In view of the fact that the present investigation indicated that the NBS of ArsA are nonequivalent and differentially affected by antimonite, we decided to reinvestigate the kinetics of ATP hydrolysis using a P_i assay initiated by mixing ArsA with MgATP/Sb(III) in a stopped-flow device (see under "Materials and Methods" for the details of the assay). This stopped-flow experiment revealed a biphasic burst in the production of P_i that resulted from ATP hydrolysis by ArsA. Following a lag in activity of about 40 ms, presumably attributable to the time taken for formation of the catalytic complex, there was a burst in P_i production over the following 100 ms (*e.g.* k = 47 s^{-1}) and a second burst was apparent over 10 s (*e.g.* k = 0.2 s^{-1}). Both bursts were of a similar amplitude, with the production of 6 and 7 μM P_i per μM of ArsA, indicating that the ArsA turns over several times before the steady-state intermediate builds up to a rate-limiting concentration. In contrast, ArsA equilibrated with Sb(III) produced a fast burst, with a similar rate constant and amplitude, but the slow burst phase was absent, being replaced by an apparent lag in activity that was most pronounced during the first 2 s of the

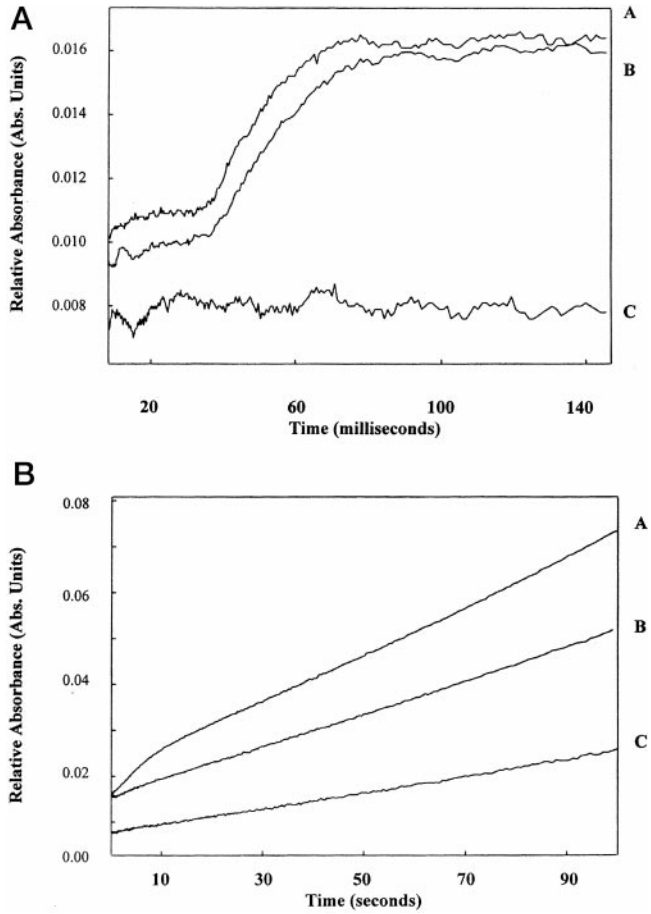

FIG. 15. **Phosphate burst phase of ArsA ATPase.** 10 μM ArsA was mixed with 1 mM ATP in a stopped-flow device, and the release of phosphate was monitored spectrophotometrically as the change in absorbance at 360 nm associated with the phosphorolysis of 2-amino-6-mercapto-7-methylpurine by phosphate. This experiment was performed in the presence of 0.5 mM Sb(III), equilibrated with either the ATP (*traces A*) or ArsA (*traces B*), or in the absence of Sb(III) (*traces C*). *A* and *B* show the production of P_i over the first 140 ms and 100 s of the reaction, respectively. Two bursts in P_i production, over 100 ms and 20 s, could be resolved when the ArsA was simultaneously mixed with ATP and Sb(III); and thereafter P_i production was linear over the next 80 s, but extended analyses established that P_i production remained linear over 1000 s. The data between 40 and 250 ms were fitted to a single-exponential function, and the data between 0.25 and 90 s were fitted to a single exponential function with a linear term. This analysis indicated that the fast and slow burst phases occurred with apparent rate constants and amplitudes of 49 (± 1) s^{-1} and 74.0 (± 0.1) μM and 0.20 (± 0.03) s^{-1} and 71 (± 1) μM, respectively, and with a steady-state release of phosphate at a rate of 6 μM^{-1} ArsA.

reaction (Fig. 15*A*, *trace B*). Furthermore, when Sb(III) was omitted from the reaction, there was no fast burst, and the slow burst was not readily apparent over this 100-s time base (Fig. 15*B*, *trace C*). Previously, in the absence of Sb(III), we noted a slow burst in P_i release of about 2 nmol P_i·nmol^{-1} ArsA, which occurred over 2000 s, with a rate constant of 0.001 s^{-1} (26). This behavior indicates that antimonite rapidly activates both NBS, so that they can hydrolyze MgATP, with several molecules undergoing hydrolysis in a burst of activity. In our previous analysis of the ATPase mechanism, we postulated that following product release, a conformational transition of the ArsA back to its original conformation was rate-limiting for steady-state ATP hydrolysis in the absence of Sb(III). The present study suggests more complex

$$\begin{array}{ccccccc} & & & & \text{ArsA*-MgADP·P}_i & & \\ & & & & k_{-r}\Uparrow k_r & & \\ \text{ArsA} + \text{MgATP} & \leftrightarrows & \text{ArsAMgATP} & \leftrightarrows & \text{ArsA-MgADP·P}_i & \leftrightarrows & \text{ArsA} + \text{MgADP} + P_i \end{array}$$

SCHEME 4

behavior because several turnovers are necessary to allow the build up of an ArsA conformation that rate-limits the steady state. An interesting possibility, which has been proposed for other ATPases (31), is the trapping of an ArsA·MgADP·P_i intermediate (Scheme 4),

If product release from ArsA occurs at a faster rate than formation of the ArsA·MgADP·P_i intermediate, then several turnovers will occur before all the ArsA becomes trapped in this state, after which subsequent turnovers will be rate-limited by the dissociation of the ArsA*-MgADP·P_i complex (*e.g.* k_{-r}). Equilibration of the ArsA with antimonite leads to further activation of the site that turns over slowly, so that MgATP turnover is no longer rate-limited by a step subsequent to hydrolysis. Indeed, the slow burst phase is replaced by an activity lag, which correlates with the time taken for the transition between the conformations stabilized by MgATP and Sb(III), respectively (27). A simple mechanism for Sb(III) to activate the ATPase would be for antimonite to cause an increase in k_{-r}, so that the ArsA*-MgADP·P_i intermediate does not build up. In the present investigation we have provided evidence that Sb(III) destabilizes an ArsA-MgADP·P_i complex, possibly ArsA*-MgADP·P_i.

DISCUSSION

Most ATP-driven efflux pumps have a quaternary structure in which there are two nucleotide-binding sites (NBS), both of which are required for ATPase and transport activity. An understanding of how these sites interact is fundamental to an understanding of the molecular events involved in the action of these pumps. Previously, we have undertaken a rigorous analysis of the kinetics of the binding of the substrate ATP to the ArsA ATPase. This analysis was facilitated using a derivative of ArsA that contains a single tryptophan residue, Trp^{159}, which is optically responsive to the binding of ATP but much less so to the binding of the product ADP (28). Herein we report on the use of another derivative of ArsA that contains a single tryptophan residue, Trp^{141}, which is more responsive to the binding of ADP than ATP (28). These tryptophan residues span the DTAP region, which connects the allosteric soft metal-binding site with the nucleotide-binding site, in the A1 half of ArsA. The binding of MgATP to Trp^{159} ArsA induces a transient increase in the tryptophan fluorescence, and we have attributed the slow decay in fluorescence to a conformational re-arrangement of ArsA that follows product release, and the protein adopts its original unliganded conformation. The binding of MgADP to Trp^{141} ArsA induces a quench in the tryptophan fluorescence; and herein we report on a detailed investigation of the kinetics of MgADP binding to Trp^{141} ArsA, and we compare this with MgATP binding to Trp^{159} ArsA.

The initial ArsA-nucleotide complexes formed with MgATP and MgADP are of a similar affinity (*cf.* 620 *versus* 600 μM), but overall ArsA has a higher affinity for MgATP over MgADP (*cf.* 430 *versus* 760 μM). In both cases, the formation of the initial complex is rate-limited by a subsequent conformational change, but is 4 orders of magnitude faster for the ArsA-MgADP complex. This isomerization, which may result from closure of the NBS, will have the effect of tightening the binding of the nucleotide, indicating apparent K_d values of 230 and 30 μM for MgATP and MgADP, respectively. We attribute the difference between these values and the measured K_d values (*e.g.* 230 *versus* 430 μM for MgATP and 760 *versus* 30 μM for MgADP) to the ArsA alternating between conformations that differ in their affinities for the Mg-nucleotide (see kinetic Scheme 2).

The two different forms of ArsA (*e.g.* $ArsA^1$ and $ArsA^2$ in Scheme 2) may represent open and closed conformations of the nucleotide-binding site (NBD). This prediction is consistent with the recently determined structure of ArsA, which revealed MgADP locked into the A1 NBD but free to diffuse from the A2 NBD (25). This is an interesting observation because in the present study we have found that MANT-ADP-induced dissociation of MgADP is rapid, with a $k_{off} > 223$ s^{-1}, but the MANT-ADP used to displace ADP might only do so at a single site, the A2 NBS. Furthermore, a 20-fold lower concentration of Mg-MANT-ADP can replace bound MgADP on ArsA, indicating that MANT-ADP is bound with higher affinity than MgADP. On the other hand, whereas the ArsA-MgMANT-ADP complex readily dissociates upon dilution, the ArsA-MgADP complex does not, and EDTA is required to dissociate the ArsA-MgADP complex, indicating that MgADP is bound more tightly than MgMANT-ADP. Furthermore, EDTA-induced dissociation of the ArsA-MgADP complex occurs at a much slower rate than k_{off} for MANT-ADP displacement (*e.g.* 6.6 s^{-1} *versus* >223 s^{-1}). A simple and reasonable explanation of this anomalous behavior is that MANT-ADP displaces ADP from the A2 NBS, whereas EDTA induces MgADP dissociation from the A1 NBS. Consistent with this interpretation, an additional fast phase is observed when MgADP is used to displace Mg·MANT-ADP from ArsA. These experiments are also consistent with earlier UV-activated nucleotide cross-linking studies that suggested that the A1 NBS is a high affinity, poorly exchangeable site, whereas the A2 NBS is a low affinity, easily exchangeable site (24). An interesting proposal is that the binding of nucleotides to the A1 and A2 sites is mutually exclusive, with, for example, the binding of nucleotide to the A1 site transiently locking the ArsA in an A1 closed/A2 open (*e.g.* $ArsA^1$) conformation.

Antimonite affects the distribution of the two different conformational forms of ArsA by preferentially stabilizing one conformation. Moreover, the kinetics of the binding of MgADP to the ArsA-Sb(III) complex strongly suggests that Sb(III) sequesters the ArsA in one of two mutually exclusive conformations (*e.g.* the $ArsA^1$-MgADP-Sb(III) complex). Most notably, the appearance of the phase attributed to formation of $ArsA^1$-MgADP-Sb(III) mirrors the disappearance of that attributed to formation of the $ArsA^2$-MgADP-Sb(III) complex (Fig. 14). The Sb(III) stabilized conformation is one in which there is enhanced and retarded release of nucleotides from the low and high affinity sites, respectively. An obvious interpretation of these data is that Sb(III) stabilizes the $ArsA^1$ conformation in which the A1 NBS is closed and the A2 NBS is open. The demonstration of both a fast and slow burst in P_i production is

consistent with two catalytic sites of high and low affinity (Fig. 15). The site that produces the slow burst is activated by Sb(III) so that ATP hydrolysis at this site is no longer rate-limited by steps subsequent to the hydrolysis step. The stabilization of the $ArsA^1$ conformation provides a mechanism for activation by stabilizing the open conformation of the A2 site, so that product dissociation from this site is no longer rate-limiting.

Interestingly, we find that the binding of Sb(III) to the ArsA-MgADP complex, and of MgATP to the ArsA-Sb(III) complex, is triphasic, and the rate of each phase is dependent upon the antimonite concentration; indicative of three ArsA-MgNucleotide-Sb(III) complexes, with K_d values of about 50, 100, and 400 μM. We previously proposed that these might be slowly inter-converting complexes, but the recent determination of the structure of the ArsA-MgADP-Sb(III) complex has revealed that three antimonite molecules are bound to ArsA in the complex. One Sb(III) is bound to His^{148} (A1) and Ser^{420} (A2), one to Cys^{113} (A1) and Cys^{422} (A2), and one to Cys^{172} (A1) and His^{453} (A2). This suggests a physical interpretation of the kinetic behavior; each antimonite complex results from the addition of an antimonite molecule to ArsA as the high, medium, and low affinity sites are successively filled. Clearly, it is tempting to speculate on whether these antimonite complexes play differential roles in controlling the affinities and activities of the A1 and A2 NBDs. Mutagenesis experiments point toward a differential role; mutation of His^{148} and His^{453} to alanines resulted in a 5-fold reduction in the affinity for metal-stimulated ATP hydrolysis,[6] whereas significantly more severe were mutations of the cysteine ligands. The $Cys^{113} \rightarrow$ Ser and $Cys^{172} \rightarrow$ Ser proteins exhibited a 20-fold increase in the concentration of antimonite required for half-maximal activation, whereas the Cys^{422}–Ser protein exhibited a 200-fold increase (33). The P_i burst experiments reported herein indicate that Sb(III) has three major effects as follows: stimulation of the A1 and A2 NBS, so that they under go a burst in P_i production during a multiple turnover event, followed by further activation of the A2 site, so that product dissociation is no longer rate-limiting. An interesting proposal is that the binding of successive antimonite molecules, which progressively increase the A1-A2 interactions, controls these events. We note that the high, intermediate, and low affinity ArsA-MgATP complexes are formed at rates that differ by more than an order of magnitude between each complex, so that they are formed successively in time. Only formation of the high affinity complex occurs at a rate that could control the fast burst phase. The rate of formation of the intermediate affinity complex, but not the low affinity complex, is sufficiently fast to control the slow burst, and formation of the low affinity complex the activation of the low affinity NBS. However, no slow burst occurs when ArsA is equilibrated with Sb(III) prior to mixing with MgATP, suggesting that the binding of the second antimonite may control activation of the low affinity NBS.

The structure and function of ArsA are suggestive of the following model of the events occurring at the NBS. In the absence of ligands, ArsA oscillates between two conformations as follows: $ArsA^1$ in which the A1 site is closed and the A2 site open, and $ArsA^2$ in which the A1 site is open and the A2 site closed. MgATP can bind to either conformation with the distribution of conformers dependent upon the affinities of the A1 and A2 sites. However, the binding of Sb(III) to the high affinity antimonite-binding site sequesters the ArsA into the $ArsA^1$ conformation. This triggers a burst in MgATP hydrolysis at the A1 site, catalyzing the build up of a pre-steady-state intermediate that rate-limits further turnover. Since Sb(III) hinders the dissociation of MgADP from the high affinity NBS, this suggests that the intermediate is ArsA-MgADP. Why should Sb(III) activate the A1 NBS? One possibility is that the hydrolysis of MgATP during the burst phase is required to drive a conformational change in the ArsA. This conformational change could involve an enhancement in the interaction of the A1 and A2 domains, possibly leading to formation of the intermediate antimonite-binding site. Similarly, the binding of Sb(III) to this site may be necessary to drive a further conformational change, activating the A2 site so that it can catalyze the rapid hydrolysis of MgATP, leading to a further tightening of the A1-A2 domain interaction and formation of the low affinity antimonite-binding site. The binding of Sb(III) to this site triggers the rapid release of product MgADP. In other words, the three Sb(III) ions "zip" the A1 and A2 domains together, 'locking' ArsA in the activated form, in which there is continuous rapid hydrolysis of MgATP at the A2 NBS. This must be coupled to the pumping of Sb(III) molecules across the membrane, but how?

The structure of ArsA indicates that the buried surface between the A1 and A2 domains is relatively small compared with the total surface of the enzyme, such that ArsA is essentially a hollow protein with a large central cavity (25). The metal-binding site is open below this central cavity, and it is sealed above by the loop between helices H9 and H10 that provide the ligand Cys^{172}. Thus, it is possible that during the catalytic cycle of ArsA antimonite ions may access the metal site from the central cavity, to then be injected into ArsB in association with a conformational change in the H9-H10 region (33). ArsA would then be similar to a "pumping heart" that expands while drawing antimonite ions from the cytoplasm and contracts while expelling them into the membrane channel provided by ArsB. To achieve this pump action, the ArsA must bind and release Sb(III) ions into the ArsB channel. The hydrolysis of MgATP at the A2 site may drive the ArsA between conformations that have high and low affinity for antimonite. In this context, we note that the affinity of ArsA for Sb(III) is increased by the binding of Mg·nucleotides. Could the three antimonite sites be used to relay the Sb(III) ion through ArsA to ArsB? The release of MgADP from the A2 NBS could trigger a reduction in the affinity of the "high affinity" binding site for Sb(III), allowing its release to ArsB, but this site can only be refilled by Sb(III) from the intermediate affinity site, and the intermediate site by Sb(III) from the low affinity site, thus providing a mechanism to draw Sb(III) into ArsA and eject it into the ArsB channel. In effect, the two P_i burst phases are required to "prime the pump" with Sb(III).

Acknowledgment—The stopped-flow instrument was purchased with grants from the University of Glasgow and the Royal Society.

REFERENCES

1. Dey, S., and Rosen, B. P. (1995) in *Drug Transport in Antimicrobial and Anticancer Chemotherapy* (Georgopapadakou, N. H., ed) pp. 103–132, Marcel Dekker, Inc., New York
2. Ambudkar, S. V., Dey, S., Hrycyna, C. A., Ramachandra, M., Pastan, I., and Gottesman, M. M. (1999) *Annu. Rev. Pharmacol. Toxicol.* **39,** 361–398
3. van Veen, H. W., and Konings, W. N. (1998) *Biochim. Biophys. Acta* **1365,** 31–36
4. Kaur, P. (1997) *J. Bacteriol.* **179,** 569–575
5. Vanden Bossche, H., Dromer, F., Improvisi, I., Lozano-Chiu, M., Rex, J. H., and Sanglard, D. (1998) *J. Med. Vet. Mycology Suppl.* **36,** 119–128
6. Borst, P., and Ouellette, M. (1995) *Annu. Rev. Microbiol.* **49,** 427–460
7. Loo, T. W., and Clarke, D. M. (1994) *J. Biol. Chem.* **269,** 7750–7755
8. Loo, T. W., and Clarke, D. M. (1995) *J. Biol. Chem.* **270,** 22957–22961
9. Sharom, F. J., Liu, R., Romsicki, Y., and Lu, P. (1999) *Biochim. Biophys. Acta* **1461,** 327–345
10. Senior, A. E. (1998) *Acta Physiol. Scand.* **163,** 213–218
11. Lerner-Marmarosh, N., Gimi, K., Urbatsch, I. L., Gros, P., and Senior, A. E. (1999) *J. Biol. Chem.* **274,** 34711–34718
12. Nagata, K., Nishitani, M., Matsuo, M., Kioka, N., Amachi, T., and Ueda, K. (2000) *J. Biol. Chem.* **275,** 17626–17630
13. Gao, M., Cui, H.-R., Loe, D. W., Grant, C. E., Almquist, K. C., Cole, S. P. C., and

[6] H. Bhattacharjee and B. P. Rosen, unpublished observations.

Deeley, R. G. (2000) *J. Biol. Chem.* **275,** 13098–13106
14. Hung, L.-W., Wang I. X., Nikaido, K., Liu, P.-Q., Ames, G. F., and Kim, S. H. (1998) *Nature* **396,** 703–707
15. Holland, I. B., and Blight, M. A. (1999) *J. Mol. Biol.* **293,** 381–399
16. Nikaido, K., and Ames, G. F. L. (1999) *J. Biol. Chem.* **274,** 26727–26735
17. Loo, T. W., and Clarke, D. M. (2000) *J. Biol. Chem.* **275,** 19435–19438
18. Conseil, G., Baubichon-Cortay H., Dayan, G., Jault, J. M., Barron, D., and DiPictro, A. (1998) *Proc. Natl. Acad. Sci. U. S. A.* **95,** 9831–9836
19. Rosen, B. P., Bhattacharjee, H., Zhou, T., and Walmsley, A. R. (1999) *Biochim. Biophys. Acta* **1461,** 207–215
20. Karkaria, C. E., Chen, C. M., and Rosen, B. P. (1990) *J. Biol. Chem.* **265,** 7832–7836
21. Kaur, P., and Rosen, B. P. (1992) *J. Biol. Chem.* **267,** 19272–19277
22. Li, J., and Rosen, B. P. (1998) *J. Biol. Chem.* **273,** 6796–6800
23. Li, J., Liu, S., and Rosen, B. P. (1996) *J. Biol. Chem.* **271,** 25247–25252
24. Kaur, P. (1999) *J. Biol. Chem.* **274,** 25849–25854
25. Zhou, T., Radaev, S., Rosen, B. P., and Gatti, D. L. (2000) *EMBO J.* **19,** 4838–4845
26. Walmsley, A. R., Zhou, T., Borges-Walmsley, M. I., and Rosen, B. P. (1999) *J. Biol. Chem.* **274,** 16153–16161
27. Walmsley, A. R., Zhou, T., Borges-Walmsley, M. I., and Rosen, B. P. (2001) *Biochemistry,* in press
28. Zhou, T., and Rosen, B. P. (1997) *J. Biol. Chem.* **272,** 19731–19737
29. Walmsley, A. R., and Bagshaw, C. R. (1989) *Anal. Biochem.* **176,** 313–318
30. Fersht, A. (1985) *Enzyme Structure and Mechanism*, pp. 139–141, W. H. Freeman & Co., New York
31. Walmsley, A. R. (2000) in *Membrane Transport: Practical Approach* (Baldwin, S. A., ed) pp. 167–192, Oxford University Press, Oxford
32. Jackson, A. P., and Bagshaw, C. R. (1988) *Biochem. J.* **251,** 527–540
33. Bhattacharjee, H., Li, J., Ksenzenko, M. Y., and Rosen, B. P. (1995) *J. Biol. Chem.* **270,** 11245–11250
34. Gatti, D. L., Mitra, B., and Rosen, B. P. (2000) *J. Biol. Chem.* **275,** 34009–34012

A Kinetic Model for the Action of a Resistance Efflux Pump

Adrian R. Walmsley, Tongqing Zhou, M. Ines Borges-Walmsley and Barry P. Rosen

J. Biol. Chem. 2001, 276:6378-6391.
doi: 10.1074/jbc.M008105200 originally published online November 28, 2000
